SIAM J. SCI. COMPUT.
Vol. 24, No. 3, pp. 732–769

RESIDUAL DISTRIBUTION SCHEMES FOR CONSERVATION LAWS VIA ADAPTIVE QUADRATURE*

RÉMI ABGRALL† AND TIMOTHY BARTH‡

Abstract. This paper considers a family of nonconservative numerical discretizations for conservation laws which retain the correct weak solution behavior in the limit of mesh refinement whenever sufficient-order numerical quadrature is used. Our analysis of 2-D discretizations in nonconservative form follows the 1-D analysis of Hou and Le Floch [*Math. Comp.*, 62 (1994), pp. 497–530]. For a specific family of nonconservative discretizations, it is shown under mild assumptions that the error arising from nonconservation is strictly smaller than the discretization error in the scheme. In the limit of mesh refinement under the same assumptions, solutions are shown to satisfy a global entropy inequality. Using results from this analysis, a variant of the "N" (Narrow) residual distribution scheme of van der Weide and Deconinck [*Computational Fluid Dynamics* '96, Wiley, New York, 1996, pp. 747–753] is developed for first-order systems of conservation laws. The modified form of the N-scheme supplants the usual exact single-state mean-value linearization of flux divergence, typically used for the Euler equations of gasdynamics, by an equivalent integral form on simplex interiors. This integral form is then numerically approximated using an adaptive quadrature procedure. This quadrature renders the scheme nonconservative in the sense described earlier so that correct weak solutions are still obtained in the limit of mesh refinement. Consequently, we then show that the modified form of the N-scheme can be easily applied to general (nonsimplicial) element shapes and general systems of first-order conservation laws equipped with an entropy inequality, where exact mean-value linearization of the flux divergence is not readily obtained, e.g., magnetohydrodynamics, the Euler equations with certain forms of chemistry, etc. Numerical examples of subsonic, transonic, and supersonic flows containing discontinuities together with multilevel mesh refinement are provided to verify the analysis.

Key words. residual distribution, fluctuation splitting, symmetric hyperbolic, entropy symmetrization

AMS subject classifications. 35L02, 65M02, 65K02, 76N02

PII. S106482750138592X

1. Motivations.

Discrete conservation has become a standard design criteria in the development of numerical discretization techniques for conservation laws that admit discontinuous solutions. From the Lax–Wendroff theorem [21], the ingredients of consistency, stability, and discrete conservation yield convergent approximations of conservation laws in *divergence form* for both smooth and discontinuous solutions that are valid weak solutions in the sense of distribution theory. Even so, the development of stabilized numerical discretizations also often utilizes the *quasi-linear form* (a.k.a. nonconservative form) of the conservation law system to approximate simple or plane wave solutions for use in upwind stabilization mechanisms. As we will illustrate later, the use of quasi-linear forms is often at odds with the requirement of discrete conservation unless specialized mean-value linearized variants of the discrete

*Received by the editors March 2, 2001; accepted for publication (in revised form) April 18, 2002; published electronically October 29, 2002. The authors gratefully acknowledge NSF/INRIA program grant INT-0072863 and INRIA research grant "Multiresolution Algorithms for Unstructured Meshes in Engineering."

http://www.siam.org/journals/sisc/24-3/38592.html

†Mathématiques Appliquées de Bordeaux, Université Bordeaux I, 351 Cours de la Libération, 33 405 Talence cedex, France (abgrall@math.u-bordeaux.fr) and Institut Universitaire de France. This research was conducted while the author was visiting RIACS, NASA Ames Research Center in 1998.

‡NASA Ames Research Center, Information Sciences Directorate, Moffett Field, CA, 94035-1000 (barth@nas.nasa.gov). The research of this author was conducted during a stay at University Bordeaux I in 2000.

quasi-linear form are used. As a practical matter, obtaining simple expressions for these mean-value linearizations in closed form is often extremely complicated or even impossible. In addressing this difficulty, our goal is to develop a general framework that avoids these complications while still ensuring that valid weak solutions of the conservation law system are obtained in the limit of mesh refinement.

As a motivating example, consider the scalar Cauchy problem in one space dimension and time,

$$\begin{cases} u_{,t} + (f(u))_{,x} = 0 \quad \text{for } (x,t) \in \mathbb{R} \times \mathbb{R}^+, \\ u(x,0) = u_0(x), \end{cases} \tag{1.1}$$

with $u \in \mathbb{R}$ and $f(u) : \mathbb{R} \mapsto \mathbb{R}$. In this equation $u_0(x)$ is assumed to be periodic or compactly supported data. Let $\Delta x_{j+1/2} = x_{j+1} - x_j$ denote a general nonuniform partitioning of space so that u_j represents the numerical approximation $u(x_j, t)$. Next, consider the prototype conservative semidiscrete scheme

$$\frac{du_j}{dt} + \frac{h_{j+1/2} - h_{j-1/2}}{\Delta x_j} = 0 \tag{1.2}$$

with $h_{j\pm1/2}$ the numerical flux. This prototype scheme is conservative in space due to the mutual telescoping of numerical fluxes. A first-order accurate upwind scheme is easily obtained via the flux function

$$h_{j+1/2}(u_j, u_{j+1}) = \frac{1}{2}\left(f(u_j) + f(u_{j+1})\right) - \frac{1}{2}|a|_{j+1/2}\left(u_{j+1} - u_j\right) \tag{1.3}$$

with $a_{j+1/2}$ an approximation of the flux Jacobian df/du at $x_{j+1/2}$. Observe that whenever the exact mean-value linearizations are used, e.g.,

$$f(u_{j+1}) - f(u_j) = \langle a \rangle_{j+1/2}\left(u_{j+1} - u_j\right), \tag{1.4}$$

so that $a_{j\pm1/2} = \langle a \rangle_{j\pm1/2}$, the first-order upwind scheme can be written equivalently as

$$\frac{\partial u_j}{\partial t} + \langle a \rangle^-_{j+1/2} \frac{u_{j+1} - u_j}{\Delta x_{j+1/2}} + \langle a \rangle^+_{j-1/2} \frac{u_j - u_{j-1}}{\Delta x_{j-1/2}} = 0. \tag{1.5}$$

Note that this discretization is nonconservative in space unless the exact mean-value linearization (1.4) is used. Nonconservative schemes of this form are known to converge to incorrect weak solutions. More precisely, Hou and Le Floch [14] have shown (in 1-D) that if the nonconservative scheme (1.5) converges, it converges to a solution of

$$u_{,t} + (f(u))_{,x} = \mu,$$

where μ is a Borel measure source term that is expected to be zero in the regions where u is smooth and concentrated where u is not smooth. The construction of an exact mean-value linearization is readily accomplished in 1-D by the general path integration

$$\begin{aligned} f(u_B) - f(u_A) &= \int_{u_A}^{u_B} df = \int_{u_A}^{u_B} a(u)\, du \\ &= \int_{\xi_A}^{\xi_B} a(u(\xi))\, \frac{du}{d\xi}\, d\xi. \end{aligned} \tag{1.6}$$

Without loss of generality, one can restrict $u(\xi)$ to the space of polynomials, P_k. A particularly convenient choice consists of P_1 linear polynomials since

$$\begin{aligned} f(u_B) - f(u_A) &= \int_{\xi_A}^{\xi_B} a(u(\xi)) \, \frac{du}{d\xi} \, d\xi \bigg|_{u(\xi)\in P_1} \\ &= \int_{\xi_A}^{\xi_B} a(u(\xi)) d\xi \bigg|_{u(\xi)\in P_1} \left(\frac{u_B - u_A}{\xi_B - \xi_A}\right) \end{aligned} \tag{1.7}$$

so that the following mean-value speed is obtained:

$$\langle a \rangle(u_A, u_B) = \frac{1}{\xi_B - \xi_A} \int_{\xi_A}^{\xi_B} a(u(\xi)) \, d\xi \bigg|_{u(\xi)\in P_1}. \tag{1.8}$$

In Harten, Lax, and van Leer [13] this expression is interpreted as an integration in state space parameterized along the line $\pi u(\xi) = u_A + \xi \, (u_B - u_A), \ \xi \in [0, 1]$:

$$\langle a \rangle(u_A, u_B) = \int_0^1 a(\pi u(\xi)) d\xi.$$

When the locations A and B are not coincident, one can equivalently interpret this as an integration in physical space, assuming the P_1 Lagrange interpolant

$$\pi u(x) = u_A + \frac{x - x_A}{x_B - x_A} \, (u_B - u_A), \quad x \in [x_A, x_B],$$

so that $\xi = \frac{x - x_A}{x_B - x_A}$ and

$$\langle a \rangle(u_A, u_B) = \frac{1}{x_B - x_A} \int_{x_A}^{x_B} a(\pi u(x)) \, dx. \tag{1.9}$$

This latter interpretation is useful since it generalizes the mean-value construction to simplices and more arbitrary regions. Next, consider an approximation of (1.9) using NQ-point numerical quadrature

$$\langle a \rangle(u_A, u_B) = \sum_{l=1}^{NQ} \omega_l \, a(\pi u(q_l)) + R_{NQ+1}, \tag{1.10}$$

where ω_l are quadrature weights, q_l are quadrature positions, and R_{NQ+1} is the numerical remainder term. This renders the scheme (1.5) nonconservative in space. In later sections, we derive (under suitable assumptions) the same result as Hou and LeFloch and are able to characterize more precisely the Borel measure μ. In particular, the dependency of μ with respect to the number of quadrature points is given. If an adequate number of quadrature points is taken, the error terms due to nonconservation are shown to be comparable to or smaller than the discretization error of the scheme. In addition, a discrete entropy inequality is formally obtained in the limit of mesh refinement. From a practical point of view, these results are important and have the following consequences:

- Exact mean-value linearization is no longer needed. This is useful when solving systems of conservation laws for which exact mean-value linearizations are not known in closed form, e.g., magnetohydrodynamics, Euler equations with certain forms of chemistry, etc.

- General finite element shapes are permitted, e.g., tetrahedra, hexahedra, prisms, pyramids. Previous exact mean-value linearizations in closed form have been restricted exclusively to simplex shapes.

The new nonconservative formulation suggests an adaptive strategy, whereby the number of quadrature points depends on the local smoothness of the numerical solution. This strategy is undertaken in section 3.

2. Background.

In this section, we briefly review a number of well-known constructions and analytical results that we utilize later in the development and analysis of our nonconservative formulations.

2.1. Conservation laws and symmetric hyperbolic forms.

Consider the Cauchy problem for m coupled conservation laws in d space dimensions and time,

$$\begin{cases} \mathbf{w}_{,t} + \sum_{i=1}^{d} \mathbf{f}^i(\mathbf{w})_{,x_i} = 0 \quad \text{for } (x,t) \in \mathbb{R}^d \times \mathbb{R}^+, \\ \mathbf{w}(x,0) = \mathbf{w}_0(x), \end{cases} \tag{2.1}$$

where $\mathbf{w} \in \mathbb{R}^m$ denotes the vector of conserved variables and $\mathbf{f}(\mathbf{w}) : \mathbb{R}^m \mapsto \mathbb{R}^{m\times d}$ a flux vector. In addition, (2.1) is assumed to be equipped with a convex entropy extension so that the additional scalar inequality holds,

$$H_{,t} + \sum_{i=1}^{d} G^i_{,x_i} \le 0, \tag{2.2}$$

with $H(\mathbf{w}) : \mathbb{R}^m \mapsto \mathbb{R}$ a convex entropy function and $G(\mathbf{w}) : \mathbb{R}^{m\times d} \mapsto \mathbb{R}^d$ the entropy flux vector for the system. Solutions of (2.1) satisfying (2.2) are generally of the following two types [22]:

- (Classical solutions) Smooth solutions satisfying the quasi-linear form of (2.1),

  $$\mathbf{w}_{,t} + \sum_{i=1}^{d} A_i(\mathbf{w})\ \mathbf{w}_{,x_i} = 0, \quad A_i(\mathbf{w}) \equiv \mathbf{f}^i_{,\mathbf{w}}. \tag{2.3}$$

  As part of the symmetrization theory for first-order conservation laws developed by Godunov [11], Mock [23], and others, it is known that the existence of a convex entropy extension ensures that the quasi-linear form (2.3) is symmetrizable via a change of variables $\mathbf{w} \mapsto \mathbf{v}$, where $\mathbf{v} = H^T_{,\mathbf{w}} \in \mathbb{R}^m$ denotes the so-called entropy variables for the system. As consequences of symmetrization theory, performing the change of variables

  $$\widetilde{A}_0 \mathbf{v}_{,t} + \sum_{i=1}^{d} \widetilde{A}_i \mathbf{v}_{,x_i} = 0 \tag{2.4}$$

  yields the matrix $\widetilde{A}_0 \equiv \mathbf{w}_{,\mathbf{v}} = (H_{,\mathbf{w},\mathbf{w}})^{-1}$ symmetric positive definite and the matrices $\widetilde{A}_i \equiv \mathbf{f}^i_{,\mathbf{v}} = A_i \widetilde{A}_0$ symmetric. For brevity, the functional dependency of the matrices A_i and $\widetilde{A}_i$ has been omitted. Motivated by the energy analysis given in subsequent sections, we assume the basic solution unknowns are the entropy $\mathbf{v}$-variables so that the shorthand notation $A_i(\mathbf{w})$ should be interpreted as $A_i(\mathbf{w}(\mathbf{v}))$. It is useful for later developments to define the real-valued matrix combination $A(\mathbf{w}, \omega) \equiv \omega_i A_i(\mathbf{w}), \omega \in \mathbb{R}^d$, and similarly the symmetric matrix $\widetilde{A}(\mathbf{w},\omega) \equiv \omega_i \widetilde{A}_i(\mathbf{w})$. Observe that symmetry of $\widetilde{A}(\mathbf{w},\omega)$ implies that $A(\mathbf{w},\omega)$ has m real eigenvalues, $\lambda_1 \le \lambda_2 \le \cdots \le \lambda_m$, and m real eigenvectors $\mathbf{r}_k(\mathbf{w},\omega) \in \mathbb{R}^m$ satisfying the standard eigenvalue problem,

$$A(\mathbf{w},\omega)\,\mathbf{r}_k(\mathbf{w},\omega) = \lambda_k(\mathbf{w},\omega)\,\mathbf{r}_k(\mathbf{w},\omega), \quad k = 1,2,\ldots,m,$$

since the identity

$$\widetilde{A}_0^{-1/2} A(\mathbf{w},\omega)\widetilde{A}_0^{1/2} = \widetilde{A}_0^{-1/2}\widetilde{A}(\mathbf{w},\omega)\widetilde{A}_0^{-1/2}$$

shows that $A(\mathbf{w},\omega)$ is similar to a real-valued symmetric matrix.

Our keen interest in the quasi-linear form (2.3) comes from its use in the construction of upwind discretizations such as variants of Godunov's method [10] utilizing approximate Riemann solvers [32, 26] and the multidimensional fluctuation splitting scheme described in the following section. Specifically, the quasi-linear form (2.3) admits nonlinear simple wave solutions of the following form for a given unit direction vector ω:

$$\mathbf{w}(x,t) = \sum_{k=1}^{m} \alpha_k \boldsymbol{\mathcal{W}}^k(\sigma_0(\omega\cdot x - \lambda_k(\boldsymbol{\mathcal{W}}^k,\omega)\,t),\omega), \quad \sigma_0(\widetilde{x}) \equiv \sigma(\tilde{x},0), \tag{2.5}$$

where $\boldsymbol{\mathcal{W}}^k(\sigma,\omega) \in \mathbb{R}^m$ satisfies the differential relation

$$\frac{d\boldsymbol{\mathcal{W}}^k}{d\sigma} = \mathbf{r}_k(\boldsymbol{\mathcal{W}}^k(\sigma,\omega),\omega) \tag{2.6}$$

for the self-similar real-valued parameter σ. In (2.5), $\alpha_k \in \mathbb{R}$ are expansion coefficients to be determined by matching initial data. When the matrix $A(\omega)$ is assumed locally independent of $\mathbf{w}$, then local plane wave solutions are obtained. Historically, mean-value linearized variants of the quasi-linear form (2.3) have been used in 1-D to construct approximate Riemann solutions [26] for eventual use in upwind discretizations. In section 2.2, we consider a multidimensional upwinding strategy which also uses plane wave information originating from a mean-value linearized form of (2.3).

- (Discontinuous solutions) Weak solutions of the divergence form (2.1) satisfying a jump condition on space-time hypersurfaces, $\mathcal{S}$, with space-time normal vector $\hat{\mathbf{n}} = (n_t, \mathbf{n}^T)^T$,

$$n_t[\mathbf{w}]_-^+ + \sum_{i=1}^{d} \mathbf{n}_i[\mathbf{f}^i]_-^+ = 0, \tag{2.7}$$

with $[\arg((x,t))]_-^+ = \lim_{\epsilon\downarrow 0}(\arg((x,t)_{\mathcal{S}} + \epsilon\,\hat{\mathbf{n}}) - \arg((x,t)_{\mathcal{S}} - \epsilon\,\hat{\mathbf{n}}))$. In section 3, a Lax–Wendroff-like theorem is presented which addresses the convergence to weak solutions of a family of nonconservative discretizations using approximate mean-value linearization.

Note that in the remainder of the paper the notation $\|\cdot\|$ will denote a pointwise norm over m variables unless otherwise indicated. When the argument is dimensionally comparable to the $\mathbf{v}$-variables, the natural norm is *not* the standard Euclidean norm $||x|| = \sqrt{\sum_{i=1}^m x_i^2}$ but rather the dimensionally consistent matrix norm [15]

$$||x||^2_{\widetilde{A}_0} \equiv x^T \widetilde{A}_0 x, \tag{2.8}$$

where $\widetilde{A}_0$ is the inverse of the Hessian matrix of the entropy, $\widetilde{A}_0 = (H_{,\mathbf{w},\mathbf{w}})^{-1}$.

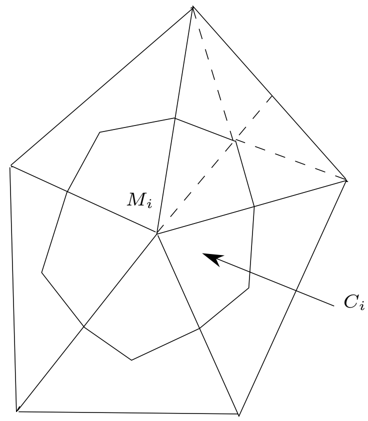

FIG. 2.1. *Dual cell C_i associated with triangulation vertex M_i in $\mathbb{R}^2$.*

2.2. The residual distribution scheme on simplices. In the remaining sections, we assume a triangulation $\mathcal{T}_h$ in $\mathbb{R}^d$ of a polygonal spatial domain Ω composed of nonoverlapping simplices T_i, $\Omega = \cup T_i$, $T_i \cap T_j = \emptyset$, $i \neq j$. A simplex T in $\mathbb{R}^d$ is uniquely described by $d+1$ vertices $T(M_1, M_2, \ldots, M_{d+1})$. For purposes of analysis, the triangulation is assumed to be shape regular with maximum simplex diameter h. From the triangulation $\mathcal{T}_h$, the geometric dual tessellation $\mathcal{C}_h$ is constructed by connecting gravity centers of the simplices and the midpoints of the edges as shown in Figure 2.1. In this figure, the dual cell C_i surrounds the triangulation vertex M_i. We also define piecewise linear and piecewise constant spaces on the tessellations $\mathcal{T}_h$ and $\mathcal{C}_h$, respectively,

$$\mathcal{V}_h = \{\mathbf{v}_h; \mathbf{v}_h \in C^0(\mathbb{R}^d)^m, \mathbf{v}_{h|T} \in (\mathcal{P}_1)^m \forall\ T \in \mathcal{T}_h\},$$

$$\mathcal{X}_h = \{\mathbf{v}_h; \mathbf{v}_{h|C} \in (\mathcal{P}_0)^m \forall\ C \in \mathcal{C}_h\}.$$

Let $\mathbf{V}_i \in \mathbb{R}^m$ denote the nodal degrees of freedom located at vertices M_i. This uniquely describes $\mathbf{v}_h$ in both spaces $\mathcal{V}_h$ and $\mathcal{X}_h$. For example, if $N_i(x)$ denotes the standard piecewise linear basis function for triangulation $\mathcal{T}_h$ such that $N_i(M_j) = \delta_{ij}$, then for $\mathbf{v}_h \in \mathcal{V}_h$, we have

$$\mathbf{v}_h(x) = \sum_{M_i \in \mathcal{T}_h} N_i(x)\, \mathbf{V}_i.$$

Similarly, if $\chi_i(x)$ denotes the characteristic function for the dual cell $C_i \in \mathcal{C}_h$,

$$\chi_i(x) = \begin{cases} 1, & x \in C_i, \\ 0, & x \notin C_i, \end{cases}$$

then for $\widetilde{\mathbf{v}}_h \in \mathcal{X}_h$, we have

$$\widetilde{\mathbf{v}}_h(x) = \sum_{M_i \in \mathcal{T}_h} \chi_i(x)\, \mathbf{V}_i.$$

Note that in these spaces we assume that the fundamental solution unknowns are the entropy $\mathbf{v}$-variables. For brevity of notation, we shall write $\mathbf{w}_h \equiv \mathbf{w}(\mathbf{v}_h)$ and

$\mathbf{W}_i \equiv \mathbf{w}(\mathbf{V}_i)$ to denote the corresponding conserved variable forms derived from the entropy variables.

Using these definitions, we can state the simplest prototype residual distribution scheme (explicit in time) used in discretizing (2.1).

Residual distribution scheme. For all $M_i \in \mathcal{T}_h$ and $n \geq 0$,

$$\begin{cases} \mathbf{W}_i^{n+1} = \mathbf{W}_i^n - \dfrac{\Delta t}{|C_i|} \sum_{T, M_i \in T} \mathbf{\Phi}_{i,T}^n, \\ \mathbf{W}_i^0 \quad = \mathbf{w}_0(M_i), \end{cases} \tag{2.9}$$

where $\mathbf{\Phi}_T \in \mathbb{R}^m$ represents a discretization of the negated time evolution term integrated in the simplex T,

$$\mathbf{\Phi}_T \equiv - \int_T (\mathbf{w}_h)_{,t} \; d\,x, \tag{2.10}$$

with $\mathbf{\Phi}_{i,T}$ an as yet unspecified sum decomposition of $\mathbf{\Phi}_T$ among the $d+1$ vertices of the simplex T in $\mathbb{R}^d$,

$$\mathbf{\Phi}_T = \mathbf{\Phi}_{1,T} + \cdots + \mathbf{\Phi}_{d+1,T}. \tag{2.11}$$

In the special case of (2.1), $\mathbf{\Phi}_T$ is expressed equivalently in terms of the spatial flux divergence,

$$\mathbf{\Phi}_T = \mathbf{\Phi}_{1,T} + \cdots + \mathbf{\Phi}_{d+1,T} = \int_T \left(\sum_{i=1}^{d} \mathbf{f}^i(\mathbf{w}_h)_{,x_i} \right) \; d\,x. \tag{2.12}$$

The residual distribution scheme encompasses a number of well-known weighted residual methods that have residual decompositions which reduce to the following form for P_1 linear elements:

$$\mathbf{\Phi}_{i,T} = \left(\frac{1}{d+1} + \overline{\tau}_{i,T} \right) \; \mathbf{\Phi}_T, \tag{2.13}$$

where $\overline{\tau}_{i,T} \in \mathbb{R}^{m \times m}$ are nonsingular matrices such that $\sum_{i=1}^{d+1} \overline{\tau}_{i,T} = 0$. Some examples of weighted residual methods for solving (2.1) include

- the streamline diffusion method of Johnson [17] and Johnson and Szepessy [18];
- the streamline upwind Petrov–Galerkin (SUPG) and Galerkin least-squares finite element methods of Hughes et al. [15, 16];
- the cell vertex finite volume methods of Ni [25] and Morton et al. [24, 7].

The residual distribution formula also describes a family of monotone and positive coefficient schemes for scalar conservation laws due to Roe [27, 28] and Deconinck, Struijs, and Roe [8] and the system extension due to van der Weide and Deconinck [31] described later in section 5. Fundamental to these residual distribution schemes is the mean-value linearization of the flux divergence formula (2.12),

$$\int_T \left(\sum_{i=1}^{d} \mathbf{f}^i(\mathbf{w})_{,x_i} \right) \; d\,x = \sum_{i=1}^{d} \langle A \rangle_i \int_T \mathbf{w}_{,x_i} \; d\,x. \tag{2.14}$$

To facilitate this calculation, we follow the 1-D example of section 1 by introducing an auxiliary mapping $\mathbf{z}(\mathbf{v}) : \mathbb{R}^m \mapsto \mathbb{R}^m$ and restricting $\mathbf{z}$ to the space of piecewise linear Lagrange interpolants denoted by $\pi_h \mathbf{z}$,

$$\int_T \left(\sum_{i=1}^{d} \mathbf{f}^i(\mathbf{w}(\pi_h \mathbf{z}))_{,x_i} \right) \, dx = \sum_{i=1}^{d} \langle A \rangle_i \int_T \mathbf{w}(\pi_h \mathbf{z})_{,x_i} \, dx. \tag{2.15}$$

For the Euler equations of gasdynamics, the choice $\mathbf{z} = (\sqrt{\rho}, \sqrt{\rho}\vec{V}, \sqrt{\rho} H_t)^T$, with ρ being the fluid density, $\vec{V}$ the fluid velocity, and H_t the fluid total enthalpy, yields closed form expressions for the mean-value linearization of the flux divergence [30]. A striking property of this linearization is that the linearized system

$$\mathbf{w}_{,t} + \sum_{i=1}^{d} \langle A \rangle_i \mathbf{w}_{,x_i} = 0 \tag{2.16}$$

is hyperbolic. Unfortunately, no other $\mathbf{z}$-variable is known to give simple and closed form formulas leading to a hyperbolic linearized system. In addition, this approach is limited to simplices, while in many applications hexahedral brick meshes would be desirable for accuracy reasons.

From a theoretical and practical point of view, there is motivation to work directly with the entropy variables since the corresponding mean-value linearized form

$$\int_T \left(\sum_{i=1}^{d} \mathbf{f}^i(\mathbf{w})_{,x_i} \right) \, dx = \sum_{i=1}^{d} \langle \widetilde{A} \rangle_i \int_T \mathbf{v}_{,x_i} \, dx \tag{2.17}$$

would necessarily produce a hyperbolic linearized system due to the symmetry of $\langle \widetilde{A} \rangle_i$. Using symmetric forms, we also show in subsequent analysis the satisfaction of an entropy inequality in the limit of mesh refinement. Our general strategy is to utilize a piecewise linear representation of the entropy variables themselves so that $\mathbf{v}_h \in \mathcal{V}_h$ and

$$\int_T \left(\sum_{i=1}^{d} \mathbf{f}^i(\mathbf{w}(\mathbf{v}_h))_{,x_i} \right) \, dx = \sum_{i=1}^{d} \langle \widetilde{A} \rangle_i \int_T (\mathbf{v}_h)_{,x_i} \, dx = |T| \sum_{i=1}^{d} \langle \widetilde{A} \rangle_i (\mathbf{v}_h)_{,x_i} \tag{2.18}$$

with

$$\langle \widetilde{A} \rangle_i \equiv \frac{1}{|T|} \int_T \widetilde{A}_i(\mathbf{v}_h) \, dx. \tag{2.19}$$

Following the 1-D motivational example of section 1, (2.19) is approximated using an NQ-point quadrature formula with weights ω and locations q so that componentwise, we have

$$\langle \widetilde{A} \rangle_i \equiv \sum_{l=1}^{NQ} \omega_l \widetilde{A}_i(\mathbf{v}_h(q_l)) + R_{NQ+1}. \tag{2.20}$$

Since $\mathbf{v}_h|_T \in P_1(T)$, (2.18) uses the fact that the gradient components are constant within a simplex. Consequently, the quadrature formula used in (2.20),

$$\int_T H(x) \, dx = |T| \sum_{l=1}^{NQ} \omega_l \, H(q_l) + O(h^{k+1}), \tag{2.21}$$

should at least be exact for $H(x) \in P_k(T)$ and $k > 1$. In addition, the $O(h^{k+1})$ error is assumed to have the following behavior for use in later analysis: There exists a C independent of the simplex T such that

$$O(h^{k+1}) \leq C(\mathcal{T}_h)\, \frac{h^{k+1}}{(k+1)!} \int_T ||D^{k+1}H(x)||\, dx, \tag{2.22}$$

where h is the maximum diameter of the T, $C(\mathcal{T}_h)$ is a geometrical parameter that depends only on $\mathcal{T}_h$, and

$$D^k H(x) = \left\{ \frac{\partial^\alpha H}{\partial x^\alpha},\ |\alpha| = k \right\}.$$

Note that the use of numerical quadrature permits generalization of the techniques to nonsimplicial elements, e.g., brick elements (Q) using the quadrature formula

$$\mathbf{\Phi}_Q = |Q| \sum_{l=1}^{NQ} \omega_q \left(\sum_{i=1}^{d} \widetilde{A}_i(\mathbf{v}_h(q_l))(\mathbf{v}_h(q_l))_{,x_i} \right) + R_{NQ+1}. \tag{2.23}$$

Returning to simplices, we are thus interested in residual distributive schemes that fulfill the approximate conservation relation

$$\mathbf{\Phi}_{1,T} + \cdots + \mathbf{\Phi}_{d+1,T} = |T| \sum_{l=1}^{NQ} \omega_q \left(\sum_{i=1}^{d} \widetilde{A}_i(\mathbf{v}_h(q_l))(\mathbf{v}_h(q_l))_{,x_i} \right). \tag{2.24}$$

In section 5, a particular residual scheme known as the N-scheme is considered [30] as generalized to systems of conservation laws by van der Weide and Deconinck [31]. This system N-scheme assumes an exact mean-value linearization via the parameter vector. We then propose a variant of the system N-scheme utilizing a piecewise linear space consisting of the entropy variables and approximating the mean-value linearization via quadrature. Analyzing this new scheme for systems of conservation laws, we show that in the limit of mesh refinement that numerical solutions satisfy an entropy inequality. We then show a similar result for the system N-scheme when the linearization is approximated via quadrature.

3. A Lax–Wendroff result for residual distribution schemes utilizing quadrature. Consider the numerical scheme (2.9). The nodal variables $\mathbf{W}_i^n$ are assumed to map uniquely via $\mathbf{v}(\mathbf{w})$ and $\mathbf{w}(\mathbf{v})$ to and from $\mathbf{V}_i^n$, which are the degrees of freedom in the spaces $\mathcal{V}_h$ and $\mathcal{X}_h$ at time $t_n \equiv n\Delta t, n \in [0, N]$. In addition, the as yet unspecified residual decompositions $\mathbf{\Phi}_{i,T}^n$ and $\mathbf{V}_i^n$ are assumed to satisfy the following conditions.

ASSUMPTION 1 (H1). *Let $\mathcal{T}_h$ be a shape regular triangulation. For $C \in \mathbb{R}$ and any fixed n, there exists $C'(C) \in \mathbb{R}$, which depends on the triangulation $\mathcal{T}_h$ such that for all $\mathbf{v}_h^n \in \mathcal{V}_h$ and $||\mathbf{v}_h^n||_{L^\infty(\mathbb{R}^d)^m} \leq C$,*

$$\left|\left|\mathbf{\Phi}_{i,T}^n\right|\right| \leq C'\, h^{d-1} \sum_{M_j \in T} \left|\left|\mathbf{V}_j^n - \mathbf{V}_i^n\right|\right| \quad \forall\, T \in \mathcal{T}_h \text{ and } \forall M_i \in T. \tag{3.1}$$

This is a continuity assumption on the residual decomposition in a simplex T in terms of the local nodal values of $\mathbf{V}_i^n, M_i \in T$. In particular, whenever $\mathbf{v}_h^n$ is constant in T, we then require that $\mathbf{\Phi}_{i,T}^n = 0$.

ASSUMPTION 2 (H2). *For all* $\mathbf{v}_h^n \in \mathcal{V}_h$ *and fixed* n

$$\mathbf{\Phi}_T^n = \sum_{i=1}^{d+1} \mathbf{\Phi}_{i,T}^n = |T| \sum_{l=1}^{NQ} \omega_l \left(\sum_{i=1}^{d} \widetilde{A}_i(\mathbf{v}_h^n(q_l))\, (\mathbf{v}_h^n(q_l))_{,x_i} \right), \quad q_l \in T, \tag{3.2}$$

where $\widetilde{A}_i = \mathbf{f}^i_{,\mathbf{v}}$ *and* NQ *denotes the number of quadrature points. In addition, the quadrature error in the flux divergence calculation is assumed to be of the following form for all* n *and a given integer* $k > 1$:

$$\left\| \mathbf{\Phi}_T^n - \int_T \sum_{i=1}^{d} \mathbf{f}^i_{,x_i}(\mathbf{v}_h^n)\, dx \right\| \le C(\mathcal{T}_h) \frac{h^{k+1}}{(k+1)!} \left\| D_x^{k+1} \left(\sum_{i=1}^{d} \widetilde{A}_i(\mathbf{v}_h^n)\, (\mathbf{v}_h^n)_{,x_i} \right)_T \right\| \tag{3.3}$$

by using a sufficient number of quadrature points.

REMARK 1.

(i) *Observe that* $\mathbf{v}_h \in \mathcal{V}_h$ *is* C^0 *continuous, consequently for neighboring simplices sharing a common spatial edge,* $\Gamma_{jk} = \{x \mid \partial T_j \cap \partial T_k \ne \emptyset\}$,

$$\sum_{i=1}^{d} \mathbf{f}^i(\mathbf{v}_h^n(x))|_{T_j} \cdot \vec{n}_i^{jk} = \sum_{i=1}^{d} \mathbf{f}^i(\mathbf{v}_h^n(x))|_{T_k} \cdot \vec{n}_i^{jk}, \quad x \in \Gamma_{jk}, \tag{3.4}$$

where $\vec{n}^{jk}$ *is a directed normal on* Γ_{jk}.

(ii) *For* $\mathbf{v}^n \in \mathcal{V}_h$ *and fixed* n *with* $||\mathbf{v}_h^n||_{L^\infty(\mathbb{R}^d)} \le C$, *there exists a* $C'(C)$ *such that for shape regular* $T \in \mathcal{T}_h$,

$$||\mathbf{\Phi}_T^n|| \le \frac{C'}{h} \sum_{M_i, M_j \in T} ||\mathbf{V}_j^n - \mathbf{V}_i^n||. \tag{3.5}$$

(iii) *Last, for any sequence* $(\mathbf{v}_h^n)_h$ *such that* $(\mathbf{v}_h^n)$ *is bounded in* $L^\infty(\mathbb{R}^d \times \mathbb{R}^+)^m$ *independently of* h *and* N *and converges in* $L^2_{loc}(\mathbb{R}^d \times \mathbb{R}^+)^m$ *to* $\mathbf{v}$, *we have*

$$\lim_{h \to 0} \left|\left| \mathbf{f}^i(\mathbf{v}_h) - \mathbf{f}^i(\mathbf{v}) \right|\right|_{L^1_{loc}(\mathbb{R}^d \times \mathbb{R}^+)^m} = 0, \quad i = 1, 2, \ldots, d. \tag{3.6}$$

Our first principal result is a generalization of the Lax–Wendroff theorem to residual distribution schemes for systems of conservation laws using numerical quadrature. Note that since the mapping $H(\mathbf{w})$ is smooth and $\mathbf{w}_h$ is bounded, assumptions on $\mathbf{w}_h$ are equivalent to the same assumptions on $\mathbf{v}_h$ defined by the nodal values $\mathbf{V}_i$.

THEOREM 3.1. *Consider initial data* $\mathbf{v}_0 \in L^\infty(\mathbb{R}^d)^m$ *and final time* $\tau > 0$. *Let* $\mathbf{W}_i$ *be the nodal approximation for all* $M_i \in \mathcal{T}_h$ *given by* (2.9) *from which* $\mathbf{V}_i$ *are obtained via* $\mathbf{V}_i \equiv \mathbf{v}(\mathbf{W}_i)$. *Assume that the scheme satisfies assumptions* (H1) *and* (H2) *and that there exists a constant* C *that depends only on* $\mathbf{v}_0$ *and functions* $\mathbf{v} \in L^2(\mathbb{R}^d \times \mathbb{R}^+)^m$ *and* $\mathbf{v}_h$ *such that for* $\mathbf{v}_h \in \mathcal{V}_h$,

$$\sup_h \sup_{x,t} ||\mathbf{v}_h(x,t)|| \le C, \quad \lim_{h \to 0} ||\mathbf{v}_h - \mathbf{v}||_{L^2_{loc}(\mathbb{R}^d \times \mathbb{R}^+)^m} = 0. \tag{3.7}$$

Let $\mathcal{Q} = \cup T$ *be a bounded domain in* $\mathbb{R}^d$, *and let* $\tau > 0$ *be a bounded time. Assume that there exists a locally bounded, positive measure* μ *such that* $||D\mathbf{v}_h||$ *tends to* μ *in the sense of distributions as* $h \to 0$. *Then* $\mathbf{v}(x,t)$ *satisfies*

$$\begin{aligned} \Bigg|\Bigg| \int_{\mathcal{Q} \times [0,\tau]} \left(\frac{\partial \varphi}{\partial t} \mathbf{w}(\mathbf{v}(x,t)) + \sum_{i=1}^{d} \frac{\partial \varphi}{\partial x_i}(x,t) \cdot \mathbf{f}^i(\mathbf{w}(\mathbf{v}(x,t))) \right) dx\, dt \\ + \int_{\mathcal{Q}} \varphi(x,0)\, \mathbf{w}(\mathbf{v}_0(x))\, dx \Bigg|\Bigg| \le \frac{C(\mathcal{T}_h, \mathbf{f})}{(k+1)!} \langle |\varphi|, \mu \rangle, \end{aligned} \tag{3.8}$$

where k is an integer as described in Assumption (H2) *and* $C(\mathcal{T}_h, \mathbf{f})$ *is a constant that depends on* $\mathcal{T}_h$ *and* $\|D_{\mathbf{v}}^{k+1}\mathbf{f}_{,\mathbf{v}}\|$.

This results applies when the limit is piecewise smooth, as it is in practical applications. The proof was inspired first by [20] and then by [2].

4. Proof of Theorem 3.1. The proof of Theorem 3.1 appeals to a sequence of lemmas that are somewhat classical but are tailored here specifically to residual distribution schemes and the use of numerical quadrature for element interior integrations. For simplicity, we assume an evolution to time τ, an N integer multiple of Δt, i.e., $\tau = N\,\Delta t$, although the generalization to arbitrary bounded positive values of τ is straightforward.

LEMMA 4.1. *Let $\mathcal{Q} = \cup T$ denote a bounded domain of $\mathbb{R}^d$, and let $\tau > 0$ be a bounded time. Further, let $(\mathbf{v}_h)_h$ denote a sequence such that $\mathbf{v}_h(\ .\ , n\Delta t) \in \mathcal{V}_h$ for any $n \le N$. Assume there exists a constant C, independent of h and N, and a function $\mathbf{v} \in L^2(\mathcal{Q} \times [0,\tau])$ such that*

$$\sup_h \sup_{x,t} ||\mathbf{v}_h(x,t)|| \le C, \quad \lim_{h\to 0} ||\mathbf{v}_h - \mathbf{v}||_{L^2_{loc}(\mathcal{Q}\times[0,\tau])^m} = 0. \tag{4.1}$$

Under these assumptions, the following limits and bound are obtained:

1. $\lim_{h\to 0}\sum_{n=0}^{N}\Delta t\sum_{\forall T\in\mathcal{Q}}|T|\sum_{M_i,M_j\in T}\left|\left|\mathbf{V}_i^n - \mathbf{V}_j^n\right|\right| = 0.$
2. $\lim_{h\to 0}\sum_{n=0}^{N}\Delta t\sum_{\forall T\in\mathcal{Q}}|T|\sum_{M_i,M_j\in T}\left|\left|\mathbf{V}_i^n - \mathbf{V}_j^n\right|\right|^2 = 0.$
3. $\lim_{h\to 0} h\ ||D_x\mathbf{v}_h||_{L^2(\mathcal{Q}\times[0,\tau])^m} = 0.$
4. *There exists C' independent of h and n such that $h||D_x\mathbf{v}_h||_{L^\infty(\mathcal{Q}\times[0,\tau])^m} \le C'$.*

Proof. To prove this lemma, one need only consider real-valued functions. The main idea of the proof relies on the observation that $\sum_{M_i,M_j\in T}||v_i - v_j||$ can be rewritten as an average over all possible cyclic permutations σ of $\{1,2,\dots,d+1\}$ of $\sum_{M_i}\left|\left|v_i - v_{\sigma(i)}\right|\right|$. Since there is a fixed finite number of such cyclic permutations, it is sufficient to prove that for any σ,

$$\lim_{h\to 0}\sum_{n=0}^{N}\Delta t\sum_{\forall T\in\mathcal{Q}}|T|\sum_{M_i\in T}\left|\left|v_i^n - v_{\sigma(i)}^n\right|\right| = 0.$$

For any simplex T and open time interval $I^n =]t_{n-1}, t_n[$, two piecewise constant functions can be constructed which are useful in analysis, namely,

$$\mathbf{v}_h(x,t)|_{T\times I^n} = \sum_{M_i\in T}\chi_{C_i\cap T}(x)\,\mathbf{V}_i^n \tag{4.2}$$

and the shifted variant

$$\widetilde{\mathbf{v}}_h(x,t)|_{T\times I^n} = \sum_{M_i\in T}\chi_{C_i\cap T}(x)\,\mathbf{V}_{\sigma(i)}^n, \tag{4.3}$$

where $\sigma(i)$ denotes a cyclic permutation of the index i and $\chi_{C_i\cap T}$ is the characteristic function of $C_i \cap T$ with C_i the dual cell at node M_i. This defines two functions on $\mathcal{Q}\times[0,\tau]$ that are bounded independently of h and N. Moreover, the following useful identity holds for these functions in a simplex T for arbitrary $p \ge 0$:

$$|T|\sum_{M_i,M_j\in T}\|\mathbf{V}_i^n - \mathbf{V}_j^n\|^p = (d+1)\int_T \|\mathbf{v}_h - \widetilde{\mathbf{v}}_h\|^p\,dx, \tag{4.4}$$

where the "$d+1$" factor comes from the definition of dual cells in $\mathbb{R}^d$. Integrating in time, we have

$$\sum_{n=0}^{N} \Delta t \sum_{\forall T \in \mathcal{Q}} |T| \sum_{M_i, M_j \in T} \|\mathbf{V}_i^n - \mathbf{V}_j^n\| = \int_0^\tau \int_{\cup T \subset \mathcal{Q}} \|\mathbf{v}_h - \widetilde{\mathbf{v}}_h\| \, dx \, dt. \tag{4.5}$$

The sequence $(\mathbf{v}_h)_h$ is bounded; therefore a function $\mathbf{v}' \in L^\infty(\mathcal{Q} \times [0,\tau])^m$ exists such that $\mathbf{v}_h \to \mathbf{v}'$ for the weak–$*$ topology. From the previous assumptions, $\mathbf{v}_h \to \mathbf{v}$ in L^2_{loc} which implies $\mathbf{v} = \mathbf{v}'$ since $\mathcal{Q} \times [0,\tau]$ is bounded and $C_0^\infty(\mathcal{Q} \times [0,\tau])$ is dense in $L^1(\mathcal{Q} \times [0,\tau])$. Similarly, there exists a function $\widetilde{\mathbf{v}} \in L^\infty(\mathcal{Q} \times [0,\tau])^m$ such that $\widetilde{\mathbf{v}}_h \to \widetilde{\mathbf{v}}$ in the weak–$*$ topology. Our next task is to show that $\widetilde{\mathbf{v}} = \mathbf{v}$ and thus finally $\widetilde{\mathbf{v}} = \mathbf{v} = \mathbf{v}'$. To do so, we let $\varphi(x,t) \in C_0^\infty(R^d \times \mathbb{R}^+)$, integrate $\varphi\, \mathbf{v}_h$ in $\mathcal{Q} \times [0,\tau]$, and use the definition of the shifted function $\widetilde{\mathbf{v}}$,

$$\begin{aligned}
\int_0^\tau \int_{\mathcal{Q}} \varphi\, \mathbf{v}_h \; dx\, dt &= \sum_{n=0}^{N} \Delta t \sum_{\forall T \in \mathcal{Q}} \sum_{M_i \in T} \mathbf{V}_i^n \int_T \varphi\, \chi_{C_i \cap T} \; dx\, dt \\
&= \int_0^T \int_{\mathcal{Q}} \varphi\, \widetilde{\mathbf{v}}_h \; dx\, dt \\
&\quad + \sum_{n=0}^{N} \Delta t \sum_{M_i \in T} \mathbf{V}_i^n \left(\int_T \varphi\, \chi_{C_i \cap T} \; dx - \int_T \varphi\, \chi_{C_{\sigma^{-1}(i)} \cap T} \; dx \right),
\end{aligned} \tag{4.6}$$

where $\sigma^{-1}(i)$ denotes the inverse cyclic index permutation such that $\sigma(\sigma^{-1}(i)) = i$. Due to the use of gravity centers and edge midpoints in the definition of the dual cells C_i, we have

$$\int_T \chi_{C_i \cap T} \; dx = \int_T \chi_{C_{\sigma^{-1}(i)}} \; dx = |C_i \cap T|, \quad i = 1, 2, \ldots, d+1. \tag{4.7}$$

Using the integral mean-value theorem, points $\overline{x}_i$ and $\overline{x}_i' \in T$ can be found such that

$$\int_T \varphi\, \chi_{C_i \cap T} \; dx = |C_i \cap T|\, \varphi(\overline{x}_i), \quad \int_T \varphi\, \chi_{C_{\sigma^{-1}(i)}} \; dx = |C_i \cap T|\, \varphi(\overline{x}_i'). \tag{4.8}$$

Since $\|D\varphi\|$ is bounded on $\mathcal{Q} \times [0,T]$ and V_h is bounded,

$$\left\| \int_0^T \int_{\mathcal{Q}} \varphi\, \mathbf{v}_h \; dx\, dt - \int_0^\tau \int_{\mathcal{Q}} \varphi\, \widetilde{\mathbf{v}}_h \; dx\, dt \right\| \le Ch, \tag{4.9}$$

where C is independent of h and N. Hence, in the limit $\widetilde{\mathbf{v}} = \mathbf{v}$ and finally $\widetilde{\mathbf{v}} = \mathbf{v} = \mathbf{v}'$.

Let v_h, $\widetilde{v}_h$, and v_h' denote scalar components of the respective vector-valued functions $\mathbf{v}_h$, $\widetilde{\mathbf{v}}_h$, and $\mathbf{v}_h'$. By the same technique, we see that the components (v_h^2) and $(\widetilde{v}_h^2)$ have the same weak–$*$ limit. It will now be shown that this limit is v^2. Once again appealing to the density of $C_0^\infty(\mathcal{Q} \times [0,\tau])$ in $L^1(\mathcal{Q} \times [0,\tau])$ and the fact that v_h^2 is bounded independently of h and N, we will take test functions φ in $C_0^\infty(\mathcal{Q} \times [0,\tau])$. The function φ is bounded in $\mathcal{Q} \times [0,\tau]$ and $v_h \to v$ in $L^2_{loc}(\mathcal{Q} \times [0,\tau])$; thus

$$\int_{\mathcal{Q} \times [0,\tau]} \varphi\, |v - v_h|^2 \; dx\, dt \to 0, \tag{4.10}$$

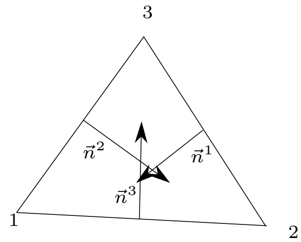

FIG. 4.1. *Depiction of inward pointing normals, $\vec{n}^i$, for a simplex in $\mathbb{R}^2$.*

and consequently,

$$\int_{\mathcal{Q}\times[0,\tau]} \varphi\, v^2 \; dx\, dt - 2\int_{\mathcal{Q}\times[0,\tau]} \varphi\, v\, v_h \; dx\, dt + \int_{\mathcal{Q}\times[0,\tau]} \varphi\, v_h^2 \; dx\, dt \to 0. \tag{4.11}$$

By the Cauchy–Schwarz inequality and $\varphi\, v \in L^1(\mathcal{Q}\times[0,\tau])$, the second term converges to

$$\int_{\mathcal{Q}\times[0,\tau]} \varphi\, v^2 \; dx\, dt. \tag{4.12}$$

Hence, $v_h^2 \to v^2$ in L^∞ weak–$*$. We are free to choose $\varphi = 1$ combined with the limit $\widetilde{v}_h^2 \to v^2$ in L^∞ weak–$*$, yielding

$$\int_{\mathcal{Q}\times[0,\tau]} |\widetilde{v}_h - v|^2 \; dx\, dt \to 0, \tag{4.13}$$

and finally,

$$\int_{\mathcal{Q}\times[0,\tau]} |\widetilde{v}_h - v_h|^2 \; dx\, dt \to 0. \tag{4.14}$$

Interpreting this equation of the form (4.4) gives the asserted limit 1 of Lemma 4.1. The limit 2 of Lemma 4.1 is then clear: $\mathcal{Q}\times[0,\tau]$ is bounded and thus $L^2(\mathcal{Q}\times[0,\tau]) \subset L^1(\mathcal{Q}\times[0,\tau])$. To prove limit 3 of Lemma 4.1, we consider Figure 4.1, which shows a simplex with inward pointing normals scaled by the edge length. In $\mathbb{R}^d$, the normal $\vec{n}^i$ is the inward pointing vector perpendicular to the $(d-1)$-dimensional simplex facet opposite vertex $M_i, i = 1, 2, \dots, d+1$, scaled by the measure of this facet so that $\sum_{i=1}^{d+1} \vec{n}^i = 0$. Using this notation, we have

$$D_x \mathbf{v}_{h|T} = \frac{1}{(d+1)\,|T|} \sum_{j=1}^{d+1} \vec{n}^j\, \mathbf{V}_j = \frac{1}{(d+1)\,|T|} \sum_{j=2}^{d+1} \vec{n}^j\, (\mathbf{V}_j - \mathbf{V}_1). \tag{4.15}$$

Integrating in time and space, we obtain

$$\begin{aligned}\sum_{n=0}^{N} \int_{I^n} \int_{\mathcal{Q}} ||D_x \mathbf{v}_h^n||^2 \; dx\, dt &= \sum_{n=0}^{N} \Delta t \sum_{\forall T\in\mathcal{Q}} |T| \left|\left|(D_x \mathbf{v}_h^n)_{|T|}\right|\right|^2 \\ &\le C \frac{1}{h^2} \sum_{n=0}^{N} \Delta t \sum_{\forall T\in\mathcal{Q}} \sum_{M_i, M_j\in T} |T| \; \left|\left|\mathbf{V}_i^n - \mathbf{V}_j^n\right|\right|^2\end{aligned}$$

because the gradient is constant within a simplex and the triangulation is regular. Limit 3 of Lemma 4.1 is then obtained from the application of limit 2. To obtain the bound 4 of Lemma 4.2, we again consider (4.15) assuming bounded $\mathbf{V}_j$,

$$\begin{aligned} &h\,||D_x\mathbf{v}_h||_{L^\infty(\mathcal{Q}\times[0,\tau])^m} \\ &\le \frac{h}{(d+1)\,|T|}\max_{1\le j\le d+1}|\vec{n}^j|\max_{1\le j\le d+1}\mathbf{V}_j \le C\frac{h}{(d+1)\,|T|}\max_{1\le j\le d+1}|\vec{n}^j|, \end{aligned} \tag{4.16}$$

which is bounded from above by a constant independent of h and N for shape regular triangulations. This concludes the proof of Lemma 4.1. ∎

LEMMA 4.2. *Let $\varphi(x,t)\in C_0^1(\mathbb{R}^d\times\mathbb{R}^+)$. With the assumptions of Theorem 3.1, we have*

$$\begin{aligned} \sum_{n=0}^{N}\sum_{M_i\in\mathcal{T}_h}|C_i|\,\varphi(M_i,t_n)\,(\mathbf{W}_i^{n+1}-\mathbf{W}_i^n) + \int_{\mathbb{R}^d\times\mathbb{R}^+}\frac{\partial\varphi}{\partial t}(x,t)\,\mathbf{w}_h(x,t)\;dx\,dt \\ + \int_{\mathbb{R}^d}\varphi(x,0)\,\mathbf{w}_0(x)\;dx\to 0 \end{aligned} \tag{4.17}$$

when $h\to 0$.

The proof is classical; see, for example, Kröner [19, p. 377].

LEMMA 4.3. *If $\mathbf{v}_h(x,t)\in\mathcal{V}_h$ satisfies the assumptions of Theorem 3.1, then for any bounded $\mathcal{Q}$ and smooth $\varphi(x,t)$,*

$$\begin{aligned} &\lim_{h\to 0}\sup_h h^{k+1}\left|\sum_{n=0}^{N}\sum_{\forall T\in\mathcal{Q}}\pi_h\varphi(x_T,t_n)\int_T\left\|D_x^{k+1}\left(\sum_{i=1}^{d}\widetilde{A}_i(\mathbf{v}_h)\,(\mathbf{v}_h)_{,x_i}\right)\right\|\;dx\right| \\ &\le\; C(\mathcal{T}_h,\mathbf{f})\,\langle|\varphi|,\mu\rangle, \end{aligned} \tag{4.18}$$

where $\pi_h\varphi(x_T,t_n)$ is the midpoint value of the linearly interpolated φ function in simplex T for constant t_n and $C(\mathcal{T}_h,\mathbf{f})$ is a bound on $\|D_{\mathbf{v}}^{k+1}\mathbf{f}_{,\mathbf{v}}(\mathbf{v}_h)\|$ for bounded $\mathbf{v}_h$.

Proof. Using the bound $\|D_{\mathbf{v}}^{k+1}\mathbf{f}_{,\mathbf{v}}\|\le C(\mathcal{T}_h,\mathbf{f})$ together with the observation that $D_x\mathbf{v}_h$ is constant in a simplex T, we have

$$\begin{aligned} h^{k+1}||D_x^{k+1}\left(\sum_{i=1}^{d}\widetilde{A}_i(\mathbf{v}_h)\,(\mathbf{v}_h)_{,x_i}\right)|| &= h^{k+1}||D_v^{k+1}\left(\sum_{i=1}^{d}\widetilde{A}_i(\mathbf{v}_h)\right)\,((\mathbf{v}_h)_{,x_i})^{k+2}|| \\ &\le h^{k+1}||D_{\mathbf{v}}^{k+1}\widetilde{A}(\mathbf{v}_h)||\;\;||D_x\mathbf{v}_h||^{k+2} \\ &\le C(\mathcal{T}_h,\mathbf{f}_{,\mathbf{v}})\,||D_x\mathbf{v}_h||. \end{aligned} \tag{4.19}$$

Using again the fact that $D_x\mathbf{v}_h$ is constant in a simplex, it follows that

$$\begin{aligned} &\left|h^{k+1}\sum_{n=0}^{N}\sum_{\forall T\in\mathcal{Q}}\pi_h\varphi(x_T,t_n)\int_T||D_x^{k+1}\widetilde{A}(\mathbf{v}_h)||\;||D_x\mathbf{v}_h||^{k+1}\;dx\right| \\ &\le\; C(\mathcal{T}_h,\mathbf{f})\sum_{n=0}^{N}\sum_{\forall T\in\mathcal{Q}}|\pi_h\varphi|(x_T,t_n)\int_T||D_x\mathbf{v}_h||\;dx \\ &=\; C(\mathcal{T}_h,\mathbf{f})\sum_{n=0}^{N}\sum_{\forall T\in\mathcal{Q}}\int_T|\pi_h\varphi|(x_T,t_n)||D_x\mathbf{v}_h||\;dx. \end{aligned} \tag{4.20}$$

The function $|\varphi|$ is bounded and continuous on a bounded domain so in the $\limsup_{h\to 0}$ limit, the right-hand-side integral in (4.20) approaches the measure-valued function $\langle|\varphi|,\mu\rangle$ which completes the proof of Lemma 4.3. $\square$

LEMMA 4.4. *Let $\varphi(x,t) \in C_0^1(\mathbb{R}^d \times \mathbb{R}^+)$ and assume that $\mathbf{v}_h$ satisfies the conditions of Theorem* 3.1. *The following measure-valued bound exists for $h \to 0$:*

$$\begin{aligned}\limsup_{h\to 0}\sup_h \Bigg\| &\sum_{n=0}^{N} \Delta t \sum_{\forall T\in\mathcal{Q}} \pi_h\varphi(x_T,t_n) \sum_{M_i\in T} \mathbf{\Phi}_{i,T}^n \\ &+ \int_{\mathbb{R}^d\times\mathbb{R}^+} \sum_{i=1}^{d} \frac{\partial\varphi}{\partial x_i}(x,t)\,\mathbf{f}^i(\mathbf{v}_h(x,t))\,dx\,dt \Bigg\| \le \frac{C(\mathcal{T}_h,\mathbf{f})}{(k+1)!}\,\langle|\varphi|,\mu\rangle,\end{aligned} \tag{4.21}$$

where $C(\mathcal{T}_h,\mathbf{f})$ is a constant that depends on $\mathcal{T}_h$ and $\|D_{\mathbf{v}}^{k+1}\mathbf{f}_{,\mathbf{v}}\|$.

Proof. Choose $\varphi(x,t)$ such that $\operatorname{supp}(\varphi) \subset \mathcal{Q}\times[0,\tau]$. Recall that $\mathbf{\Phi}_T^n = \sum_{i=1}^{d+1}\mathbf{\Phi}_{i,T}^n$ represents an approximation of the flux divergence integrated in a simplex T. By direct calculation,

$$\sum_{n=0}^{N} \Delta t \sum_{\forall T\in\mathcal{Q}} \pi_h\varphi(x_T,t_n)\left(\sum_{i=1}^{d+1}\mathbf{\Phi}_{i,T}^n + \epsilon_h^{(k)}\right) \tag{4.22}$$

$$\begin{aligned}&= \sum_{n=0}^{N} \Delta t \sum_{\forall T\in\mathcal{Q}} \int_T \pi_h\varphi(x_T,t_n) \sum_{i=1}^{d} \mathbf{f}^i_{,x_i}(\mathbf{v}_h)\,dx \\ &= \sum_{n=0}^{N} \Delta t \sum_{\forall T\in\mathcal{Q}} \int_T \pi_h\varphi(x,t_n) \sum_{i=1}^{d} \mathbf{f}^i_{,x_i}(\mathbf{v}_h)\,dx\end{aligned}$$

$$+\sum_{n=0}^{N} \Delta t \sum_{\forall T\in\mathcal{Q}} \int_T \left(\pi_h\varphi(x_T,t_n) - \pi_h\varphi(x,t_n)\right) \sum_{i=1}^{d} \mathbf{f}^i_{,x_i}(\mathbf{v}_h)\,dx, \tag{4.23}$$

where $\epsilon_h^{(k)}$ is the quadrature error in calculating the flux divergence. From Assumption (H2), this quadrature error is assumed to be of the form

$$\begin{aligned}\|\epsilon_h^{(k)}\| &= \left\|\int_T \sum_{i=1}^{d} \mathbf{f}^i_{,x_i}(\mathbf{v}_h^n)\,dx - \sum_{i=1}^{d+1}\mathbf{\Phi}_{i,T}^n\right\| \\ &\le\ C(\mathcal{T}_h)\frac{h^{k+1}}{(k+1)!}\left\|D_x^{k+1}\left(\sum_{i=1}^{d}\widetilde{A}_i(\mathbf{v}_h^n)\,(\mathbf{v}_h^n)_{,x_i}\right)\right\|\end{aligned} \tag{4.24}$$

consequently for $\pi_h\varphi(x,t)$ bounded by a constant absorbed into $C(\mathcal{T}_h)$

$$\begin{aligned}&\left\|\sum_{n=0}^{N} \Delta t \sum_{\forall T\in\mathcal{Q}} \pi_h\varphi(x_T,t_n)\,\epsilon_h^{(k)}\right\| \\ &\le\ C(\mathcal{T}_h)\frac{h^{k+1}}{(k+1)!}\sum_{n=0}^{N}\Delta t\left\|D_x^{k+1}\left(\sum_{i=1}^{d}\widetilde{A}_i(\mathbf{v}_h^n)\,(\mathbf{v}_h^n)_{,x_i}\right)\right\|.\end{aligned} \tag{4.25}$$

Combining this result with Lemma 4.3 formally bounds the quadrature error term

$$\limsup_{h\to 0}\left|\sum_{n=0}^{N} \Delta t \sum_{\forall T\in\mathcal{Q}} \pi_h\varphi(x_T,t_n)\,\epsilon_h^{(k)}\,dx\right| \le \frac{C(\mathcal{T}_h,\mathbf{f})}{(k+1)!}\,\langle|\varphi|,\mu\rangle. \tag{4.26}$$

Next, apply Green's formula in each simplex to the first right-hand-side sum appearing in (4.23),

$$\sum_{n=0}^{N} \Delta t \sum_{\forall T \in \mathcal{Q}} \int_T \pi_h \varphi(x,t_n) \sum_{i=1}^{d} \mathbf{f}^i_{,x_i}(\mathbf{v}_h)\ dx \tag{4.27}$$

$$= \sum_{n=0}^{N} \int_{I^n} \sum_{\forall T \in \mathcal{Q}} \int_T \pi_h \varphi(x,t_n) \sum_{i=1}^{d} \mathbf{f}^i_{,x_i}(\mathbf{v}_h)\ dx\, dt$$

$$= - \sum_{n=0}^{N} \int_{I^n} \sum_{\forall T \in \mathcal{Q}} \int_T \sum_{i=1}^{d} \frac{\partial \pi_h \varphi}{\partial x_i} \mathbf{f}^i(\mathbf{v}_h)\ dx\, dt$$

$$+ \sum_{n=0}^{N} \int_{I^n} \sum_{\forall T \in \mathcal{Q}} \int_{\partial T} \pi_h \varphi(x,t_n) \sum_{i=1}^{d} \mathbf{f}^i(\mathbf{v}_h) \cdot n_i\ dx\, dt. \tag{4.28}$$

Recall that $\pi_h\varphi$ and $\mathbf{f}$ are both bounded and continuous functions. Upon utilizing Remark 1 (i) and the compact support of φ, it follows that the second right-hand-side sum of (4.28) vanishes identically. Examining the remaining right-hand-side term in (4.28), observe that

$$\left\| \sum_{n=0}^{N} \int_{I^n} \sum_{\forall T \in \mathcal{Q}} \int_T \left(\sum_{i=1}^{d} \frac{\partial \pi_h \varphi}{\partial x_i} \mathbf{f}^i(\mathbf{v}_h) - \sum_{i=1}^{d} \frac{\partial \varphi}{\partial x_i} \mathbf{f}^i(\mathbf{v}) \right) dx\, dt \right\|$$

$$\leq\ C_0 \sum_{n=0}^{N} \int_{I^n} \sum_{\forall T \in \mathcal{Q}} \int_T ||\mathbf{f}(\mathbf{v}_h) - \mathbf{f}(\mathbf{v})||\ dx\, dt$$

$$+\ C_1 \sum_{n=0}^{N} \int_{I^n} \sum_{\forall T \in \mathcal{Q}} \int_T ||D_x \pi_h \varphi - D_x \varphi||\ ||\mathbf{f}(\mathbf{v}_h)||\ dx\, dt. \tag{4.29}$$

The first right-hand-side sum of (4.29) is equal to $||\mathbf{f}(\mathbf{v}_h) - \mathbf{f}(\mathbf{v})||_{L^1(\mathcal{Q}\times[0,\tau])}$ and converges to 0 as $h \to 0$; see Remark 1 (iii). Since $\mathbf{v}_h$ stays bounded and $\mathbf{f}$ continuous, $\mathbf{f}(\mathbf{v}_h)$ stays bounded by a constant. The second right-hand-side sum of (4.29) is bounded from above by $||D_x\pi_h\varphi - D_x\varphi||_{L^1(\mathcal{Q}\times[0,\tau])}$, which also converges to 0 as $h \to 0$. Thus, we conclude that

$$\lim_{h\to 0} \left\| \sum_{n=0}^{N} \int_{I^n} \sum_{\forall T \in \mathcal{Q}} \int_T \left(\sum_{i=1}^{d} \frac{\partial \pi_h \varphi}{\partial x_i} \mathbf{f}^i(\mathbf{v}_h) - \sum_{i=1}^{d} \frac{\partial \varphi}{\partial x_i} \mathbf{f}^i(\mathbf{v}) \right) dx\, dt \right\| = 0 \tag{4.30}$$

and, consequently,

$$\begin{aligned} &\lim_{h\to 0} \sum_{n=0}^{N} \Delta t \sum_{\forall T \in \mathcal{Q}} \int_T \pi_h \varphi(x,t_n) \sum_{i=1}^{d} \mathbf{f}^i_{,x_i}(\mathbf{v}_h)\ dx \\ &= \ - \sum_{n=0}^{N} \int_{I^n} \sum_{\forall T \in \mathcal{Q}} \int_T \sum_{i=1}^{d} \frac{\partial \varphi}{\partial x_i} \mathbf{f}^i(\mathbf{v})\, dx\, dt. \end{aligned} \tag{4.31}$$

Considering the second right-hand-side sum term in (4.23), from Remark 1 (ii) it follows that

$$\left\| \sum_{n=0}^{N} \Delta t \sum_{\forall T \in \mathcal{Q}} \int_T (\pi_h \varphi(x_T,t_n) - \pi_h \varphi(x,t_n)) \sum_{i=1}^{d} \mathbf{f}^i_{,x_i}(\mathbf{v}^n_h)\ dx \right\| \leq \Sigma,$$

where

$$\Sigma \equiv C \sum_{n=0}^{N} \Delta t \sum_{\forall T \in \mathcal{Q}} \int_T \left| \frac{\pi_h \varphi(x_T, t_n) - \pi_h \varphi(x, t_n)}{h} \right| \sum_{M_i, M_j \in T} \left\| \mathbf{V}_j^n - \mathbf{V}_i^n \right\| \, dx. \tag{4.32}$$

Since $||D_x \pi_h \varphi||$ is assumed bounded by a constant,

$$\int_T \left| \frac{\pi_h \varphi(x_T, t_n) - \pi_h \varphi(x, t_n)}{h} \right| \, dx = \int_T \left| D_x \left(\pi_h \varphi \right) \cdot \frac{x_T - x}{h} \right| \, dx \le C \, h^d,$$

where C is independent of h. Inserting this bound yields

$$\begin{aligned} &\left\| \sum_{n=0}^{N} \Delta t \sum_{\forall T \in \mathcal{Q}} \int_T \left| \pi_h \varphi(x_T, t_n) - \pi_h \varphi(x, t_n) \right| \, \sum_{i=1}^{d} \mathbf{f}^i_{,x_i}(\mathbf{v}_h^n) \, dx \right\| \\ &\le \; C h^d \sum_{n=0}^{N} \Delta t \sum_{\forall T \in \mathcal{Q}} \sum_{M_i, M_j \in T} \left\| \mathbf{V}_j^n - \mathbf{V}_i^n \right\| \end{aligned} \tag{4.33}$$

so that

$$\lim_{h \to 0} \left\| \sum_{n=0}^{N} \Delta t \sum_{\forall T \in \mathcal{Q}} \int_T \left(\pi_h \varphi(x_T, t_n) - \pi_h \varphi(x, t_n) \right) \, \sum_{i=1}^{d} \mathbf{f}^i_{,x_i}(\mathbf{v}_h^n) \, dx \right\| = 0. \tag{4.34}$$

Rearrangement of the bounded terms as $h \to 0$ together with Lemma 4.1 completes the proof of Lemma 4.4. $\square$

Proof of Theorem 3.1. Multiply (2.9) by $\varphi(M_i, t_n) \, |C_i|$, where $\varphi(x, t)$ is a test function in $C_0^1 \left(\mathbb{R}^d \times [0, +\infty[\right)$, such that $\operatorname{supp}(\varphi) \subset \mathcal{Q} \times [0, \tau]$. Summation on the indices n and i over time slabs and vertices, respectively, yields

$$\begin{aligned} &\sum_{n=0}^{N} \sum_{M_i \in \mathcal{T}_h} |C_i| \, \varphi(M_i, t_n) \, \left(\mathbf{W}_i^{n+1} - \mathbf{W}_i^n \right) \\ &+ \sum_{n=0}^{N} \Delta t \sum_{M_i \in \mathcal{T}_h} \sum_{T; M_i \in T} \varphi(M_i, t_n) \, \mathbf{\Phi}^n_{i,T} = 0. \end{aligned} \tag{4.35}$$

From Lemma 4.2,

$$\begin{aligned} &\lim_{h \to 0} \sum_{n=0}^{N} \sum_{M_i \in \mathcal{T}_h} |C_i| \, \varphi(M_i, t_n) \, \left(\mathbf{W}_i^{n+1} - \mathbf{W}_i^n \right) \\ &= \; - \int_{\mathbb{R}^d \times \mathbb{R}^+} \frac{\partial \varphi}{\partial t} \, \mathbf{w}(\mathbf{v}_h(x, t)) \, dx - \int_{\mathbb{R}^d} \varphi(x, 0) \, \mathbf{w}(\mathbf{v}_0(x)) \, dx. \end{aligned}$$

The space term is rewritten

$$\begin{aligned} \sum_{n=0}^{N} \Delta t \sum_{M_i \in \mathcal{T}_h} \sum_{T; M_i \in T} \varphi(M_i, t_n) \, \mathbf{\Phi}^n_{i,T} &= \sum_{n=0}^{N} \Delta t \sum_{\forall T \in \mathcal{Q}} \sum_{M_i \in T} \pi_h \varphi(x_T, t_n) \, \mathbf{\Phi}^n_{i,T} \\ &+ \sum_{n=0}^{N} \Delta t \sum_{\forall T \in \mathcal{Q}} \sum_{M_i \in T} \left(\varphi(M_i, t_n) - \pi_h \varphi(x_T, t_n) \right) \mathbf{\Phi}^n_{i,T}, \end{aligned} \tag{4.36}$$

where once again $\pi_h\varphi(x_T, t_n)$ denotes the midpoint value of the linearly interpolated φ function for constant t_n. Examining the first right-hand-side sum of (4.36), recall the result of Lemma 4.4,

$$\limsup_{h\to 0}\sup_h \left\{ \sum_{n=0}^{N} \Delta t \sum_{\forall T\in\mathcal{Q}} \sum_{M_i\in T} \pi_h\varphi(x_T, t_n)\mathbf{\Phi}^n_{i,T} \right.$$
$$\left. + \int_{\mathbb{R}^d\times\mathbb{R}^+} \sum_{i=1}^{d} \frac{\partial\varphi}{\partial x_i}(x,t)\,\mathbf{f}^i(\mathbf{v}_h(x,t))\; dx\, dt \right\} \le \frac{C(\mathcal{T}_h, \mathbf{f})}{(k+1)!}\langle|\varphi|, \mu\rangle.$$

Next, examine the second right-hand-side sum of (4.36). From boundedness of $\|D\varphi\|$ combined with Assumption (H1), we have

$$\left|\left|\mathbf{\Phi}^n_{i,T}\right|\right| \le C'\; h^{d-1} \sum_{M_j\in T} \left|\left|\mathbf{V}^n_j - \mathbf{V}^n_i\right|\right|, \tag{4.37}$$

yielding

$$\begin{aligned}
&\left|\left| \sum_{n=0}^{N} \Delta t \sum_{\forall T\in\mathcal{Q}} \sum_{M_i\in T} (\varphi(M_i, t_n) - \pi_h\varphi(x_T, t_n))\,\mathbf{\Phi}^n_{i,T} \right|\right| \\
&\le\; Ch \sum_{n=0}^{N} \Delta t \sum_{\forall T\in\mathcal{Q}} \sum_{M_i\in T} \|\mathbf{\Phi}^n_{T,i}\| \\
&\le\; Ch^d \sum_{n=0}^{N} \Delta t \sum_{\forall T\in\mathcal{Q}} \sum_{M_i, M_j\in T} \|\mathbf{V}^n_j - \mathbf{V}^n_i\|.
\end{aligned} \tag{4.38}$$

Consequently, from Lemma 4.1, as $h \to 0$,

$$\left|\left| \sum_{n=0}^{N} \Delta t \sum_{\forall T\in\mathcal{Q}} \sum_{M_i\in T} (\varphi(M_i, t_n) - \pi_h\varphi(x_T, t_n))\,\mathbf{\Phi}^n_{i,T} \right|\right| \to 0, \tag{4.39}$$

which completes the proof of Theorem 3.1. $\square$

5. The "N" residual distribution scheme. An important example of a residual distribution scheme is the "N" (Narrow) scheme. It was first considered by Roe [27, 28] and Deconinck [8] for scalar equations. Here we consider the system extension due to van der Weide and Deconinck [31] and generalize their scheme to symmetrizable conservation laws

$$\mathbf{w}(\mathbf{v})_{,t} + \sum_{i=1}^{d} \mathbf{f}^i(\mathbf{w}(\mathbf{v}))_{,x_i} = 0. \tag{5.1}$$

Repeating (2.18) of section 2.2, our general strategy is to utilize a piecewise linear representation of the entropy variables themselves so that $\mathbf{v}_h \in \mathcal{V}_h$. In a simplex T,

$$\int_T \left(\sum_{i=1}^{d} \mathbf{f}^i(\mathbf{w}(\mathbf{v}_h))_{,x_i} \right)\; dx = \sum_{i=1}^{d} \langle \widetilde{A}_i \rangle \int_T (\mathbf{v}_h)_{,x_i}\; dx = |T| \sum_{i=1}^{d} \langle \widetilde{A}_i \rangle_T (\mathbf{v}_h)_{,x_i,|_T}, \tag{5.2}$$

with

$$\langle \widetilde{A}_i \rangle = \sum_{l=1}^{NQ} \omega_l \, \widetilde{A}_i(\mathbf{v}_h(q_l)), \qquad q_l \in T, \tag{5.3}$$

computed using NQ-point numerical quadrature. For purposes of analysis, it is convenient to define the symmetric matrices $\widetilde{K}_{j,T} \in \mathbb{R}^{m\times m}$,

$$\widetilde{K}_{j,T} \equiv \frac{1}{d+1} \sum_{i=1}^{d} \vec{n}^{j}_{i,T} \langle \widetilde{A}_i \rangle_T \quad \forall M_j \in T, \tag{5.4}$$

where $\vec{n}^j_T \in \mathbb{R}^d$ are the inward pointing normal vectors of the face of simplex T opposite vertex M_j scaled by the integral measure of the face; see, for example Figure 4.1. Also define $\widetilde{K}^{\pm} = (\widetilde{K} \pm |\widetilde{K}|)/2$, where $|\widetilde{K}|$ is calculated in the usual matrix sense via eigensystem decomposition. Due to the scaling of vector normals, $\sum_{\forall M_j \in T} \vec{n}^j_T = 0$. Consequently, we have that $\sum_{\forall M_j \in T} \widetilde{K}_{j,T} = 0$, and the identity

$$\sum_{\forall M_j \in T} \widetilde{K}^{+}_{j,T} = - \sum_{\forall M_j \in T} \widetilde{K}^{-}_{j,T}. \tag{5.5}$$

For the set of matrices $\{\widetilde{A}_i\}$ equal to the Jacobian matrices of the Euler equations evaluated at a single state, it is shown in [1] that $\left(\sum_{\forall M_j \in T} \widetilde{K}^{+}_{j}\right)$ is nonsingular everywhere except when the state corresponds to a stagnation point. More generally, if we define (formally) the matrix $N \in \mathbb{R}^{m\times m}$ in a simplex T,

$$N_T = \left(\sum_{\forall M_j \in T} \widetilde{K}^{+}_{j} \right)^{-1}, \tag{5.6}$$

it is shown in [1] that the matrix product $\widetilde{K}_j N \; \forall M_j \in T$ appearing in the N-scheme is well behaved, even at stagnation points. Hence, from now on we assume that the matrix N_T always exists in the sense just described.

Using these definitions, one can easily derive the following relationship for $\mathbf{\Phi}_T$:

$$\mathbf{\Phi}_T = \int_T \left(\sum_{i=1}^{d} \mathbf{f}^i(\mathbf{w}(\mathbf{v}_h))_{,x_i} \right) \, d\,x = |T| \sum_{i=1}^{d} \langle \widetilde{A}_i \rangle_T (\mathbf{v}_h)_{,x_i,|_T} = \sum_{\forall M_j \in T} \widetilde{K}_{j,T} \mathbf{V}_j. \tag{5.7}$$

Fundamental to the N-scheme is the following decomposition formula for $\mathbf{\Phi}_T$:

$$\mathbf{\Phi}_{j,T} = \widetilde{K}^{+}_{j,T} \, (\mathbf{V}_j - \mathbf{V}^{\text{inflow}}_T) \quad \forall M_j \in T, \tag{5.8}$$

which is often called "upwind" because it represents a generalization to $\mathbb{R}^d$ of two-point upwind differencing for model scalar advection. Perhaps, surprisingly, the requirement that $\mathbf{\Phi}_{j,T}$ represent a decomposition of $\mathbf{\Phi}_T$, i.e.,

$$\mathbf{\Phi}_T = \sum_{\forall M_j \in T} \mathbf{\Phi}_{j,T} = \sum_{\forall M_j \in T} \widetilde{K}_{j,T} \mathbf{V}_j, \tag{5.9}$$

uniquely determines $\mathbf{V}_T^{\text{inflow}}$ when N_T exists:

$$\mathbf{V}_T^{\text{inflow}} = -N_T \sum_{\forall M_i \in T} \widetilde{K}_{i,T}^{-} \mathbf{V}_i. \tag{5.10}$$

After some rearrangement, the N-scheme decomposition formula can be written in the following compact form:

$$\mathbf{\Phi}_{i,T} = \widetilde{K}_{i,T}^{+} N_T \sum_{\forall M_j \in T} \widetilde{K}_{j,T}^{-} (\mathbf{V}_j - \mathbf{V}_i) \quad \forall M_i \in T. \tag{5.11}$$

The N-scheme then evolves the solution in time using the algorithm given earlier by (2.9). We repeat this algorithm as follows while taking care to indicate the underlying dependence on $\mathbf{v}_h$ and the nodal degrees of freedom $\mathbf{V}$ that describe $\mathbf{v}_h$.

N-scheme in symmetrization variables. For all $M_i \in \mathcal{T}_h$, $n \geq 0$, and $\mathbf{v}_h \in \mathcal{V}_h$,

$$\begin{cases} \mathbf{W}_i^{n+1} = \mathbf{W}_i^n - \dfrac{\Delta t}{|C_i|} \sum_{T, M_i \in T} \mathbf{\Phi}_{i,T}(\mathbf{v}_h^n), & \mathbf{V}_i^{n+1} = \mathbf{v}(\mathbf{W}_i^{n+1}), \\ \mathbf{W}_i^0 = \mathbf{w}(\mathbf{v}_0(M_i)). \end{cases} \tag{5.12}$$

The primary interest in the N-scheme for approximating conservation laws centers around a local discrete maximum principle exhibited by the N-scheme for scalar advection equations in $\mathbb{R}^d$. To see this, let v_h, V_i, and W_i denote the scalar ($m = 1$) forms of $\mathbf{v}_h$, $\mathbf{V}_i$, and $\mathbf{W}_i$, respectively. Consider a numerical solution at steady state $v_h^n = v_h^{n+1} = v_h^*$. From (5.11), the nodal degree of freedom at vertex M_i satisfies

$$0 = \sum_{\forall T \in \mathcal{T}_h; M_i \in T} \; \sum_{M_j \in T; M_j \neq M_i} -\widetilde{K}_{i,T}^{+} N_T \widetilde{K}_{j,T}^{-} (V_j^* - V_i^*) \tag{5.13}$$

$$= \sum_{\forall T \in \mathcal{T}_h; M_i \in T} \; \sum_{M_j \in T; M_j \neq M_i} \alpha^{ij} (V_i^* - V_j^*), \quad \alpha^{ij} \geq 0. \tag{5.14}$$

This latter equation implies a local discrete maximum principle. More precisely, let $\text{adj}_\alpha(M_i)$ denote the set of vertices adjacent to M_i with nonzero weights α; then for all $M_i \in \mathcal{T}_h$,

$$\min_{M_j \in \text{adj}_\alpha(M_i)} V_j^* \leq V_i^* \leq \max_{M_j \in \text{adj}_\alpha(M_i)} V_j^*.$$

Examining the time-dependent problem in the scalar ($m = 1$) case, one easily derives a similar maximum principle result for $n > 0$,

$$\min_{M_j \in \text{adj}_\alpha(M_i)} (V_j^n, V_i^n) \leq V_i^{n+1} \leq \max_{M_j \in \text{adj}_\alpha(M_i)} (V_j^n, V_i^n),$$

under the CFL-like condition at each t_n,

$$\Delta t \leq \max_{\forall M_i \in \mathcal{T}_h} \frac{|C|_i}{\sum_{\forall T \in \mathcal{T}_h; M_i \in T} \sum_{M_j \in T; M_j \neq M_i} -\widetilde{K}_{i,T}^{+} N_T \widetilde{K}_{j,T}^{-}}.$$

6. Energy and entropy analysis of the system N-scheme. In this section, we begin with an energy analysis of the system ($m \geq 1$) N-scheme assuming a linear (constant coefficient) form of (2.4) using techniques described earlier in Barth [5]. Using results from this analysis, we then analyze the N-scheme for nonlinear systems of conservation laws with convex entropy extension. In this case, an entropy function serves as a measure of energy for the nonlinear system. This latter nonlinear analysis shows that the N-scheme using symmetrization variables and numerical quadrature satisfies an entropy inequality in the limit of mesh refinement.

6.1. Energy analysis of the system N-scheme: The linear case. In the linear (constant coefficient) system case, the numerical scheme (5.12) can be viewed abstractly as an Euler explicit integration of the semidiscrete matrix equation,

$$D\,\mathbf{V}_{,t} + L\,\mathbf{V} = 0, \tag{6.1}$$

where $\mathbf{V} \in \mathbb{R}^s$ is a vector representing the s nodal degrees of freedom, $D \in \mathbb{R}^{s\times s}$ a symmetric positive definite (SPD) matrix, and $L \in \mathbb{R}^{s\times s}$ a general real-valued matrix. The energy evolution equation is then given by

$$\frac{1}{2}(\mathbf{V}^T D\,\mathbf{V})_{,t} + \mathbf{V}^T \widetilde{L}\,\mathbf{V} = 0, \quad \widetilde{L} = (L + L^T)/2, \tag{6.2}$$

where $\widetilde{L}$ denotes the symmetric part of L. Energy boundedness is demonstrated if it can be shown that the symmetric part of L is positive semidefinite, i.e., for all $\mathbf{V}$,

$$\mathbf{V}^T \widetilde{L}\,\mathbf{V} = \mathbf{V}^T L\,\mathbf{V} \geq 0. \tag{6.3}$$

Now suppose that this abstract matrix equation originates from a discretization procedure such as the N-scheme. The total energy associated with the matrix L can be computed and assembled on an element-by-element basis,

$$\mathbf{V}^T \widetilde{L}\,\mathbf{V} = \sum_{T\in\mathcal{T}_h} \mathbf{V}_T^T \widetilde{L}_T\,\mathbf{V}_T, \tag{6.4}$$

where $\mathbf{V}_T$ and L_T denote the nodal degrees of freedom and element matrix associated with a simplex T. To demonstrate energy boundedness of the abstract linear system it is sufficient, but not necessary, to show

$$\mathbf{V}_T^T \widetilde{L}_T\,\mathbf{V}_T \geq 0 \quad \forall T \in \mathcal{T}_h. \tag{6.5}$$

We turn our attention now to the N-scheme. For ease of exposition, we will show the development in two space dimensions, but the generalization to $\mathbb{R}^d$ will be clear. Next, consider the linear (constant coefficient) form of (2.4). In this linear model, the conservation and symmetrization variables are related by the constant matrix $\widetilde{A}_0$, i.e.,

$$\mathbf{W}_i = \widetilde{A}_0\,\mathbf{V}_i \quad \forall M_i \in \mathcal{T}_h. \tag{6.6}$$

The SPD matrix D appearing in (6.1) would then be block diagonal with $m\times m$ blocks corresponding to each vertex M_i of the form $|C|_i \widetilde{A}_0$. In two space dimensions, the system N-scheme decomposition (5.11) reduces to the following space discretization for a simplex T with local numbering $T(M_1, M_2, M_3)$:

(6.7)

$$L_T \mathbf{V}_T = \begin{pmatrix} \mathbf{\Phi}_1 \\ \mathbf{\Phi}_2 \\ \mathbf{\Phi}_3 \end{pmatrix} = \left[\begin{bmatrix} \widetilde{K}_1^+ & & \\ & \widetilde{K}_2^+ & \\ & & \widetilde{K}_3^+ \end{bmatrix} + \begin{bmatrix} \widetilde{K}_1^+ \\ \widetilde{K}_2^+ \\ \widetilde{K}_3^+ \end{bmatrix} [N] \begin{bmatrix} \widetilde{K}_1^- \\ \widetilde{K}_2^- \\ \widetilde{K}_3^- \end{bmatrix}^T \right] \begin{pmatrix} \mathbf{V}_1 \\ \mathbf{V}_2 \\ \mathbf{V}_3 \end{pmatrix}$$

with $\widetilde{K}^\pm$ symmetric and $[N]$ a block diagonal matrix $[N] \equiv \mathrm{diag}(N, N, N)$. The symmetric part of L is given by

(6.8)

$$\widetilde{L}_T = \begin{bmatrix} \widetilde{K}_1^+ & & \\ & \widetilde{K}_2^+ & \\ & & \widetilde{K}_3^+ \end{bmatrix} + \frac{1}{2} \begin{bmatrix} \widetilde{K}_1^+ \\ \widetilde{K}_2^+ \\ \widetilde{K}_3^+ \end{bmatrix} [N] \begin{bmatrix} \widetilde{K}_1^- \\ \widetilde{K}_2^- \\ \widetilde{K}_3^- \end{bmatrix}^T + \frac{1}{2} \begin{bmatrix} \widetilde{K}_1^- \\ \widetilde{K}_2^- \\ \widetilde{K}_3^- \end{bmatrix} [N] \begin{bmatrix} \widetilde{K}_1^+ \\ \widetilde{K}_2^+ \\ \widetilde{K}_3^+ \end{bmatrix}^T .$$

Examining rows of L_T or $\widetilde{L}_T$, observe that the row sum is nonzero. However, we can add the following block diagonal matrix to the element matrix L:

$$-\frac{1}{2}\begin{bmatrix} \widetilde{K}_1 & & \\ & \widetilde{K}_2 & \\ & & \widetilde{K}_3 \end{bmatrix} \tag{6.9}$$

so that rows and columns of the L_T sum to zero. These additional terms have no impact on the constant coefficient discretization of the Cauchy problem. The added terms all vanish identically when summed for all elements sharing a mesh vertex since the geometry surrounding the vertex is closed. Hence, from now on we will include these terms in our definition of L_T and $\widetilde{L}_T$, yielding

(6.10)

$$\widetilde{L}_T = \frac{1}{2}\begin{bmatrix} |\widetilde{K}|_1 & & \\ & |\widetilde{K}|_2 & \\ & & |\widetilde{K}|_3 \end{bmatrix} + \frac{1}{2}\begin{bmatrix} \widetilde{K}_1^+ \\ \widetilde{K}_2^+ \\ \widetilde{K}_3^+ \end{bmatrix} [N] \begin{bmatrix} \widetilde{K}_1^- \\ \widetilde{K}_2^- \\ \widetilde{K}_3^- \end{bmatrix}^T + \frac{1}{2}\begin{bmatrix} \widetilde{K}_1^- \\ \widetilde{K}_2^- \\ \widetilde{K}_3^- \end{bmatrix} [N] \begin{bmatrix} \widetilde{K}_1^+ \\ \widetilde{K}_2^+ \\ \widetilde{K}_3^+ \end{bmatrix}^T .$$

Next, rewrite an off-diagonal term such as

$$\widetilde{K}_i^+ N \widetilde{K}_j^- + \widetilde{K}_i^- N \widetilde{K}_j^+$$

in the following form:

$$\widetilde{K}_i^+ N \widetilde{K}_j^- + \widetilde{K}_i^- N \widetilde{K}_j^+ = \widetilde{K}_i N \widetilde{K}_j - \widetilde{K}_i^+ N \widetilde{K}_j^+ - \widetilde{K}_i^- N \widetilde{K}_j^- .$$

Consequently, $\widetilde{L}_T$ can be rewritten as

$$\begin{aligned} \widetilde{L}_T &= \frac{1}{2}\begin{bmatrix} \widetilde{K}_1 \\ \widetilde{K}_2 \\ \widetilde{K}_3 \end{bmatrix} [N] \begin{bmatrix} \widetilde{K}_1 \\ \widetilde{K}_2 \\ \widetilde{K}_3 \end{bmatrix}^T \\ &+ \frac{1}{2}\begin{bmatrix} \widetilde{K}_1^+ & & \\ & \widetilde{K}_2^+ & \\ & & \widetilde{K}_3^+ \end{bmatrix} - \begin{bmatrix} \widetilde{K}_1^+ \\ \widetilde{K}_2^+ \\ \widetilde{K}_3^+ \end{bmatrix} [N] \begin{bmatrix} \widetilde{K}_1^+ \\ \widetilde{K}_2^+ \\ \widetilde{K}_3^+ \end{bmatrix}^T \\ &+ \frac{1}{2}\begin{bmatrix} -\widetilde{K}_1^- & & \\ & -\widetilde{K}_2^- & \\ & & -\widetilde{K}_3^- \end{bmatrix} - \begin{bmatrix} -\widetilde{K}_1^- \\ -\widetilde{K}_2^- \\ -\widetilde{K}_3^- \end{bmatrix} [N] \begin{bmatrix} -\widetilde{K}_1^- \\ -\widetilde{K}_2^- \\ -\widetilde{K}_3^- \end{bmatrix}^T . \end{aligned} \tag{6.11}$$

Note that the first term appearing on the right-hand side of (6.11) gives rise to a quadratic form with positive energy, so our only concern is the remaining terms on the right-hand side of this equation. Before proving positive semidefiniteness of (6.11), we first review a simple result concerning the spectra of noncommuting matrices.

LEMMA 6.1. *The nonzero parts of the spectrum of AB and BA are identical for all matrices $A \in \mathbb{R}^{m\times n}$ and $B \in \mathbb{R}^{n\times m}$.*

Proof. For the proof, see, for example, Axelsson [3, p. 69]. □

Next we prove positive semidefiniteness of a specialized matrix in product form.

LEMMA 6.2 (Golub [12]). *The matrix*

$$L = \begin{bmatrix} A & 0 & 0 \\ 0 & B & 0 \\ 0 & 0 & C \end{bmatrix} - \begin{bmatrix} A \\ B \\ C \end{bmatrix} N \begin{bmatrix} A \\ B \\ C \end{bmatrix}^T, \quad N = [A+B+C]^{-1},$$

is positive semidefinite for all $A, B, C \in \mathbb{R}^{n\times n}$ *symmetric positive definite.*

Proof. Let

$$Z = \begin{bmatrix} A & 0 & 0 \\ 0 & B & 0 \\ 0 & 0 & C \end{bmatrix},$$

and congruence transform L,

$$Z^{-1/2} L Z^{-1/2} = \begin{bmatrix} I_n & & \\ & I_n & \\ & & I_n \end{bmatrix} - \begin{bmatrix} A^{1/2} \\ B^{1/2} \\ C^{1/2} \end{bmatrix} N \begin{bmatrix} A^{1/2} \\ B^{1/2} \\ C^{1/2} \end{bmatrix}^T = I_{3n} - P.$$

Next use Lemma 6.1 concerning the spectra of nonsquare matrix products. In the present case, Lemma 6.1 implies that

$$\begin{aligned} &\text{Eigenvalues}\left(\begin{bmatrix} A^{1/2} \\ B^{1/2} \\ C^{1/2} \end{bmatrix} N \begin{bmatrix} A^{1/2} \\ B^{1/2} \\ C^{1/2} \end{bmatrix}^T \right) \\ &\quad = \text{Eigenvalues}\Big(N^{1/2}(A+B+C)N^{1/2}\Big) + 2n \text{ zeros} \\ &\quad = \text{Eigenvalues}\Big(N(A+B+C)\Big) + 2n \text{ zeros} \\ &\quad = \text{Eigenvalues}(I_n) + 2n \text{ zeros} \end{aligned} \tag{6.12}$$

and, consequently,

$$I_{3n} - P$$

is positive semidefinite. From this result, it follows immediately that

$$L = Z^{1/2}(I_{3n} - P)Z^{1/2}$$

is also positive semidefinite. ∎

The extension to $A, B, C \geq 0$ and $(A + B + C) > 0$ follows by considering the perturbed matrices $A_\epsilon = A + \epsilon I$, $B_\epsilon = B + \epsilon I$, and $C_\epsilon = C + \epsilon I$, and by letting $\epsilon \downarrow 0$.

Returning to the system N-scheme, we now can prove the main result of this section.

THEOREM 6.3. *The system N-scheme discretization of the constant coefficient form of* (2.4) *is energy bounded with the element energy matrix* (6.11) *positive semidefinite, i.e.,* $\mathbf{V}^T \widetilde{L} \mathbf{V} \geq 0$.

Proof. Since $N = [\widetilde{K}_1^+ + \widetilde{K}_2^+ + \widetilde{K}_3^+]^{-1} = [-\widetilde{K}_1^- - \widetilde{K}_2^- - \widetilde{K}_3^-]^{-1}$, the result follows immediately after application of the Golub lemma to (6.11) together with (6.4). ∎

6.2. Energy and entropy analysis of the system N-scheme: The nonlinear case. In this section, an energy analysis of the N-scheme is presented for nonlinear systems of conservation laws. This energy also represents an approximation to the entropy inequality equation (2.2); see Hughes, Franca, and Mallet [15] or Barth [6, 4] for related entropy analysis of finite element discretizations. Specifically, we show convergence to an entropy inequality for the N-scheme with exact integration.

We then show that with sufficient-order numerical quadrature the entropy inequality is retained in the limit of mesh refinement.

LEMMA 6.4. *Under the assumptions of Theorem* 3.1*, the limit* $\mathbf{v}$ *of* $\mathbf{v}_h$ *defined by the conservative system N-scheme satisfies the following integral form of* (2.2)*:*

$$\frac{d}{dt}\int_\Omega H(\mathbf{v}) + \int_{\partial\Omega}\sum_{i=1}^{d} G^i(\mathbf{v})\,\vec{n}_i\; dS \le 0. \tag{6.13}$$

Proof. Consider the system N-scheme decomposition (6.7). Unlike the constant coefficient linear case, the diagonal term (6.9),

$$-\frac{1}{2}\begin{bmatrix} \widetilde{K}_1 & & \\ & \widetilde{K}_2 & \\ & & \widetilde{K}_3 \end{bmatrix},$$

cannot be added to the element matrix L_T in the nonlinear case without changing the discretization. Consequently, the energy associated with the simplex $T(M_1,\ldots,M_{d+1})$ must include this term, i.e.,

$$\mathbf{V}_T^T\widetilde{L}_T\mathbf{V}_T = \frac{1}{2}\sum_{i=1}^{d+1}\mathbf{V}_i^T\widetilde{K}_i\mathbf{V}_i + Q(\mathbf{V}_1,\ldots,\mathbf{V}_{d+1}), \tag{6.14}$$

where the quadratic form Q is positive by Theorem 6.3. The task is to show that, in the limit $h \to 0$, the first right-hand-side term appearing in (6.14) converges to

$$\int_{\partial\Omega}\sum_{i=1}^{d} G^i(\mathbf{v})\,\vec{n}_i\; dS, \tag{6.15}$$

the integral of the entropy flux. Recall that $\mathbf{V}$ describes the nodal degrees of freedom in the piecewise linear space $\mathbf{v}_h \in \mathcal{V}_h$. By exploiting the identity $\sum_{j=1}^{d+1}\widetilde{K}_j = 0$ in a simplex T, we have the following relationship for an arbitrary $k \in \{1,\ldots,d+1\}$:

$$\sum_{j=1}^{d+1}\mathbf{V}_j^T K_j\mathbf{V}_j = \sum_{j=1, j\neq k}^{d+1}\left(\mathbf{V}_j^T\widetilde{K}_j\mathbf{V}_j - \mathbf{V}_k^T\widetilde{K_j}\mathbf{V}_k\right) \tag{6.16}$$

$$= \sum_{j=1, j\neq k}^{d+1}(\mathbf{V}_j+\mathbf{V}_k)^T\widetilde{K}_j(\mathbf{V}_j-\mathbf{V}_k) \tag{6.17}$$

$$= \sum_{j=1, j\neq k}^{d+1}(\mathbf{V}_j+\mathbf{V}_k)^T\widetilde{K}_j\,(\vec{l}^{jk}\cdot D\mathbf{v}_h), \tag{6.18}$$

where $\vec{l}^{jk}$ denotes the vector from vertex M_k to vertex M_j. Thus we can define (by identification) a vector $\mathbf{P} \in R^{m\times d}$ for each simplex T such that for an arbitrary $k \in \{1,\ldots,d+1\}$,

$$\sum_{j=1}^{d+1}\mathbf{V}_j^T K_j\mathbf{V}_j = \sum_{l=1}^{d}\mathbf{P}_l\frac{\partial\mathbf{v}_h}{\partial x_l}, \quad \mathbf{P} = \sum_{j=1, j\neq k}^{d+1}(\mathbf{V}_j+\mathbf{V}_k)^T\widetilde{K}_j\,\vec{l}^{jk}.$$

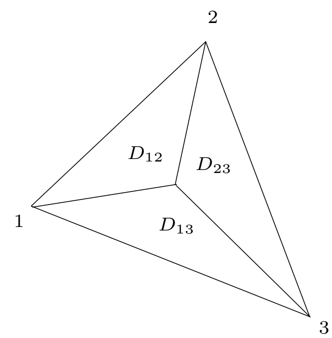

FIG. 6.1. *Geometrical elements for the definition of* w.

Using this result, we obtain

$$\frac{1}{2}\sum_{j=1}^{d}\mathbf{V}_j^T\widetilde{K}_j\mathbf{V}_j=\int_T \mathbf{v}_h\cdot\left(\sum_{l=1}^{d}\widetilde{A}_l(\mathbf{v}_h)\frac{\partial \mathbf{v}_h}{\partial x_l}\right)\,dx+\epsilon_T=\int_T\sum_{i=1}^{d}G^i_{,x_i}\,dx+\epsilon_T, \tag{6.19}$$

where G is the entropy flux associated with $\mathbf{v}$ and

$$\epsilon_T=\int_T\left(\left[\sum_{l=1}^{d}\frac{\mathbf{P}_l}{|T|}\cdot\frac{\partial \mathbf{v}_h}{\partial x_l}\right]-\mathbf{v}_h^T\left[\sum_{l=1}^{d}\widetilde{A}_l(\mathbf{v}_h)\frac{\partial \mathbf{v}_h}{\partial x_l}\right]\right)\,dx. \tag{6.20}$$

Hence, ϵ_T can be estimated,

$$\begin{aligned}|\epsilon_T|&\le\left\{\int_T\left(\sum_{l=1}^{d}\left[\frac{\mathbf{P}_l}{|T|}-\mathbf{v}_h^T\,\widetilde{A}_l(\mathbf{v}_h)\right]\right)^2dx\right\}^{1/2}\left\{\int_T||D\mathbf{v}_h||^2dx\right\}^{1/2}\\&\le\left\{\int_T\left(\sum_{l=1}^{d}\left[\frac{\mathbf{P}_l}{|T|}-\mathbf{v}_h^T\,\widetilde{A}_l(\mathbf{v}_h)\right]\right)^2dx\right\}^{1/2}\int_T||D\mathbf{v}_h||\,dx\end{aligned}$$

because $D\mathbf{v}_h$ is *constant* in each simplex T. Proceeding as in Lemma 4.1, we see that the function w defined by (see Figure 6.1 for a 2-D illustration)

$$w_{|T}=\sum_{[i,j]\text{ edge of }T}(\mathbf{V}_i+\mathbf{V}_j)\,\chi_{D_{ij}},$$

where χ_D is the characteristic function of the set D converges in $L^2_{loc}$to $2\mathbf{v}$ when $h\to 0$. Using the definition of $\widetilde{K}_j$, we have for an arbitrary $k\in\{1,\dots,d+1\}$

$$\sum_{j=1,j\neq k}^{d+1}\widetilde{K}_j(\mathbf{V}_j-\mathbf{V}_k)=|T|\,\sum_{l=1}^{d}\widetilde{A}_l\frac{\partial \mathbf{v}_h}{\partial x_l}.$$

Thus we see that

$$\sum_{l=1}^{d}\left(\sum_{j=1,j\neq k}^{d+1}\widetilde{K}_l l_l^{\vec{j}k}\right)\frac{\partial \mathbf{v}_h}{\partial x_l}=|T|\,\sum_{l=1}^{d}\widetilde{A}_l\frac{\partial \mathbf{v}_h}{\partial x_l}. \tag{6.21}$$

Due to the boundedness of $\mathbf{v}_h$, we can apply the dominated convergence theorem and (6.21), thus yielding

$$\left\{ \int_{\mathcal{Q}\times[0,\tau]} \left(\sum_{l=1}^{d} \left[\frac{\mathbf{P}_l}{|T|} - \mathbf{v}_h^T \ \widetilde{A}_l(\mathbf{v}_h) \right] \right)^2 dx \right\}^{1/2} \to 0$$

for any bounded domain $\mathcal{Q} \subset \mathbb{R}^d$. ∎

THEOREM 6.5. *Under the assumptions of Theorem* 3.1*, the limit* $\mathbf{v}$ *of* $\mathbf{v}_h$ *defined by the system N-scheme satisfies the entropy inequality*

$$\int_\Omega \frac{\partial \varphi}{\partial t} H(\mathbf{v})\, dx + \int_{\mathbb{R}^d \times \mathbb{R}^+} \sum_{i=1}^{d} \frac{\partial \varphi}{\partial x_i} G^i(\mathbf{v})\, dx + \int_{\mathbb{R}^d} \varphi(x,0)\, \mathbf{v}(x,0)\, dx \le 0 \tag{6.22}$$

for any smooth $\varphi \ge 0$.

Proof. The first observation is

$$\varphi \, \frac{dH(\mathbf{v})}{dt} = \varphi \, \mathbf{v} \cdot \frac{d\mathbf{w}}{dt}. \tag{6.23}$$

The second observation is that in a simplex $T(M_1, \dots, M_{d+1})$,

$$\sum_{i=1}^{d+1} \varphi_i \mathbf{V}_i^T \mathbf{\Phi}_i = \varphi_G \sum_{i=1}^{d+1} \mathbf{V}_i^T \mathbf{\Phi}_i + \sum_{i=1}^{d+1} (\varphi_i - \varphi_G) \mathbf{V}_i^T \mathbf{\Phi}_i, \tag{6.24}$$

where $\varphi_G = \frac{\varphi_1 + \varphi_2 + \varphi_3}{3}$. Then consequently,

$$\sum_{j=1}^{d+1} \mathbf{V}_j^T \mathbf{\Phi}_j = \frac{1}{2} \sum_{j=1}^{d+1} \mathbf{V}_j^T \widetilde{K}_j \mathbf{V}_j + Q(\mathbf{V}_1, \dots, \mathbf{V}_{d+1}), \tag{6.25}$$

where Q is positive by Theorem 6.3. Thus we observe that, because $\varphi_j, \varphi_G \ge 0$,

$$\sum_{i=1}^{d+1} \varphi_i \mathbf{V}_i^T \mathbf{\Phi}_i \ge \varphi_G \frac{1}{2} \sum_{j=1}^{d+1} \mathbf{V}_j^T \widetilde{K}_j \mathbf{V}_j + \sum_{i=1}^{d+1} (\varphi_i - \varphi_G) \mathbf{V}_i^T \mathbf{\Phi}_i. \tag{6.26}$$

The last observation is that, in a simplex T,

$$\left|\left| \sum_{i=1}^{d+1} (\varphi_i - \varphi_G) \mathbf{V}_i^T \mathbf{\Phi}_i \right|\right| \le C\, h \, ||D\varphi||_\infty \sum_{i,j=1}^{d+1} ||\mathbf{V}_i|| \ ||C_{ij}|| \ ||\mathbf{V}_i - \mathbf{V}_j|| \,, \tag{6.27}$$

where C is a constant depending on the mesh only and $C_{ij} = \widetilde{K}_i^+ N \widetilde{K}_j^-$. From this we conclude that

$$\left|\left| \sum_{i=1}^{d+1} (\varphi_i - \varphi_G) \mathbf{V}_i^T \mathbf{\Phi}_i \right|\right| \le C' h^2 \, ||D\varphi||_\infty \ ||\mathbf{V}_i - \mathbf{V}_j|| \,, \tag{6.28}$$

where C' depends on $\max_i ||\mathbf{v}_h||$ which is uniformly bounded by assumption. Since the mesh is regular, $h^2 \le C''|T|$ for a well-chosen constant independent of the mesh. Lemma 4.1 shows that the right-hand side vanishes when $h \to 0$. Using the same arguments as in Theorem 3.1 and Lemma 6.4, we conclude that the semidiscrete scheme satisfies an entropy inequality. □

Combining the previous results of this section, we finally conclude with the following corollary.

COROLLARY 6.6. *Under the assumptions of Theorem* 3.1 *and Theorem* 6.5*, the system N-scheme associated with the quadrature formula* (2.20) *satisfies in the limit* $h \to 0$ *an entropy inequality for any smooth* $\varphi \geq 0$*,*

(6.29)
$$\int_\Omega \frac{\partial \varphi}{\partial t} H(\mathbf{v}) dx + \int_{\mathbb{R}^d \times \mathbb{R}^+} \sum_{i=1}^d \frac{\partial \varphi}{\partial x_i} G^i(\mathbf{v})\ dx + \int_{\mathbb{R}^d} \varphi(x,0)\,\mathbf{v}(x,0)\ dx \leq C \frac{1}{(k+1)!} \langle |\varphi|, \mu \rangle.$$

REMARK 2. *The results of Theorem* 6.5 *and Corollary* 6.6 *state that there is an entropy inequality in the limit of a mesh refinement and sufficiently high order quadrature. In contrast, Theorem* 6.3 *states that the N-scheme for constant coefficient systems with suitable time integration is energy stable on all meshes. In general, it would be desirable to obtain a similar result for nonlinear systems on all meshes.*

7. Numerical results. In this section, numerical validation of Theorem 3.1 is provided via N-scheme calculation of smooth and discontinuous solutions of a scalar conservation law and system Euler equations for subsonic, transonic, and supersonic flows. Recall that Theorem 3.1 states, under classical assumptions, that numerical solutions of the N-scheme with adaptive quadrature converge to a function for which the residual

$$\int_{\mathcal{Q} \times [0,\tau]} \left(\phi_{,t} \mathbf{w}(x,t) + \sum_{i=1}^d \phi_{,i} \mathbf{f}_i(\mathbf{w}(x,t)) \right) dx dt + \int_{\mathcal{Q}} \phi(x,0) \mathbf{w}_0(x) dx$$

may not vanish as in the classical Lax–Wendroff theorem. Instead, the residual is bounded by a measure-valued function that can be made arbitrarily small by making the number of quadrature points sufficiently large. As a practical matter, as will be shown in section 7.1, the convergence is very rapid when derivatives of the flux components, $\mathbf{f}^i$, are well behaved. In addition, an adaptive quadrature scheme is proposed and tested, which greatly reduces the computational cost of the N-scheme with quadrature. The adaptive quadrature strategy uses a simple estimate of solution smoothness to select the number of quadrature points, thus producing an overall economical discretization method since most elements need only use one interior quadrature point (even for second-order accurate extensions [1]).

7.1. 1-D conservation law. Consider the scalar Cauchy problem (1.1)

$$\begin{cases} u_{,t} + (f(u)_{,x} = 0 & \text{for } (x,t) \in \mathbb{R} \times \mathbb{R}^+, \\ u(x,0) = u_0(x). \end{cases}$$

First, observe that the upwind scheme (1.5) of section 1 on a uniform mesh can be rewritten as

$$\Delta x_j \frac{du_j}{dt} + \left(\Phi^+_{j-1/2} + \Phi^-_{j+1/2} \right) = 0, \tag{7.1}$$

with

$$\Phi^-_{j+1/2} = \langle a \rangle^-_{j+1/2} (u_{j+1} - u_j), \quad \Phi^+_{j+1/2} = \langle a \rangle^+_{j+1/2} (u_{j+1} - u_j), \tag{7.2}$$

and from section 1,

$$\langle a\rangle_{j+1/2} \equiv \frac{f(u_{j+1})-f(u_j)}{u_{j+1}-u_j} = \int_0^1 a(\pi u(\xi))\,d\xi, \quad \pi u(\xi) = u_j + \xi\,(u_{j+1}-u_j). \tag{7.3}$$

Note that, on a nonuniform mesh, Δx_j is replaced by the lumped average $\Delta x_j = (\Delta x_{j-1/2} + \Delta x_{j+1/2})/2$ although other definitions are possible, e.g., $\Delta x_j = (p^+_{j-1/2}\,\Delta x_{j-1/2} + p^-_{j+1/2}\,\Delta x_{j+1/2})$, $p^{\pm}_{j\mp 1/2} \equiv (1 \pm \mathrm{sgn}(\langle a\rangle_{j\mp 1/2}))/2$. Consistent with the previous analysis, our first numerical experiment implements a variant of this residual distribution upwind scheme of the form

$$\Delta x_j\,\frac{du_j}{dt} + \left(\Psi^+_{j-1/2} + \Psi^-_{j+1/2}\right) = 0, \tag{7.4}$$

with residual distribution calculated via numerical quadrature,

$$\Psi^-_{j+1/2} = \sum_{l=1}^{NQ} \omega_l\, a(\pi u(q_l))^-(u_{j+1}-u_j), \quad \Psi^+_{j+1/2} = \sum_{l=1}^{NQ} \omega_l\, a(\pi u(q_l))^+(u_{j+1}-u_j). \tag{7.5}$$

The scheme (7.4) would be conservative if

$$\Psi^-_{j+1/2} + \Psi^+_{j+1/2} = f(u_{j+1}) - f(u_j),$$

but due to the use of numerical quadrature,

$$\begin{aligned}\Psi^-_{j+1/2} + \Psi^+_{j+1/2} &= \sum_{l=1}^{NQ} \omega_l\, a(\pi u(q_l))\,(u_{j+1}-u_j)\\ &\neq \int_0^1 a(\pi u(\xi))\,d\xi\,(u_{j+1}-u_j) = f(u_{j+1}) - f(u_j).\end{aligned}$$

Even so, from Theorem 3.1 we still expect convergence to weak solutions, provided sufficient order numerical quadrature is employed.

7.1.1. 1-D numerical experiment: Fixed Gauss quadrature on nonuniform mesh. We first test the scheme (7.4) with Euler explicit time advancement for the smooth flux formula and initial data,

$$f(u) = e^u, \quad u_0(x) = \sin(2\pi x),$$

on successively refined meshes ($\Delta x = 10^{-2}$, $(1/2)\ 10^{-2}$, $(1/2)^2\ 10^{-2}$, $(1/2)^3\ 10^{-2}$, and $(1/2)^4\ 10^{-2}$). To eliminate superconvergent behavior of measured error norms due to mesh uniformity, we make the spacing between successive mesh points alternate between the values Δx and $\Delta x/2$. In evaluating the distribution formulas (7.5), NQ-point Gauss quadrature formulas are used with $1 \le NQ \le 3$ to validate Theorem 3.1. Selected results are given in Table 7.1, which tabulates L^1, L^2, and L^∞ norms of the difference between the numerical solution u^n_c given by standard conservative scheme (7.1) and the nonconservative u^n_{nc} provided by the scheme (7.4) on meshes with decreasing Δx at time $n\Delta t = 0.5$ (after the shockwave has appeared). Figures 7.1(a)–(d) graph the solutions before and after the occurrence of the shockwave for the conservative and nonconservative schemes using 1, 2, 3, 4, and 5 point Gauss

TABLE 7.1
Numerical results for the 1-D Cauchy problem. Numerical error between the conservative calculation u_c and the nonconservative calculation u_{nc} using NQ-point Gauss quadrature.

Mesh size, Δx	$L^1(u_{nc} - u_c)$	$L^2(u_{nc} - u_c)$	$L^\infty(u_{nc} - u_c)$	#quad pts, NQ
$0.100\ 10^{-1}$	0.6353110^{-2}	$0.25617\ 10^{-1}$	0.15162	1
$0.500\ 10^{-2}$	$0.67850\ 10^{-2}$	$0.38770\ 10^{-1}$	0.35783	1
$0.250\ 10^{-2}$	$0.70532\ 10^{-2}$	$0.55376\ 10^{-1}$	0.67416	1
$0.125\ 10^{-2}$	$0.72127\ 10^{-2}$	$0.73250\ 10^{-1}$	$0.10491\ 10^{1}$	1
$0.100\ 10^{-1}$	$0.12402\ 10^{-4}$	$0.50233\ 10^{-4}$	$0.30796\ 10^{-3}$	2
$0.500\ 10^{-2}$	$0.14468\ 10^{-4}$	$0.83082\ 10^{-4}$	$0.74799\ 10^{-3}$	2
$0.250\ 10^{-2}$	$0.15648\ 10^{-4}$	$0.12657\ 10^{-3}$	$0.14325\ 10^{-2}$	2
$0.125\ 10^{-2}$	$0.16296\ 10^{-4}$	$0.18732\ 10^{-3}$	$0.33085\ 10^{-2}$	2
$0.100\ 10^{-1}$	$0.28748\ 10^{-7}$	$0.42536\ 10^{-7}$	$0.23256\ 10^{-6}$	3
$0.500\ 10^{-2}$	$0.27937\ 10^{-7}$	$0.44600\ 10^{-7}$	$0.35562\ 10^{-6}$	3
$0.250\ 10^{-2}$	$0.27315\ 10^{-7}$	$0.48398\ 10^{-7}$	$0.49170\ 10^{-6}$	3
$0.125\ 10^{-2}$	$0.27017\ 10^{-7}$	$0.57222\ 10^{-7}$	$0.93983\ 10^{-6}$	3

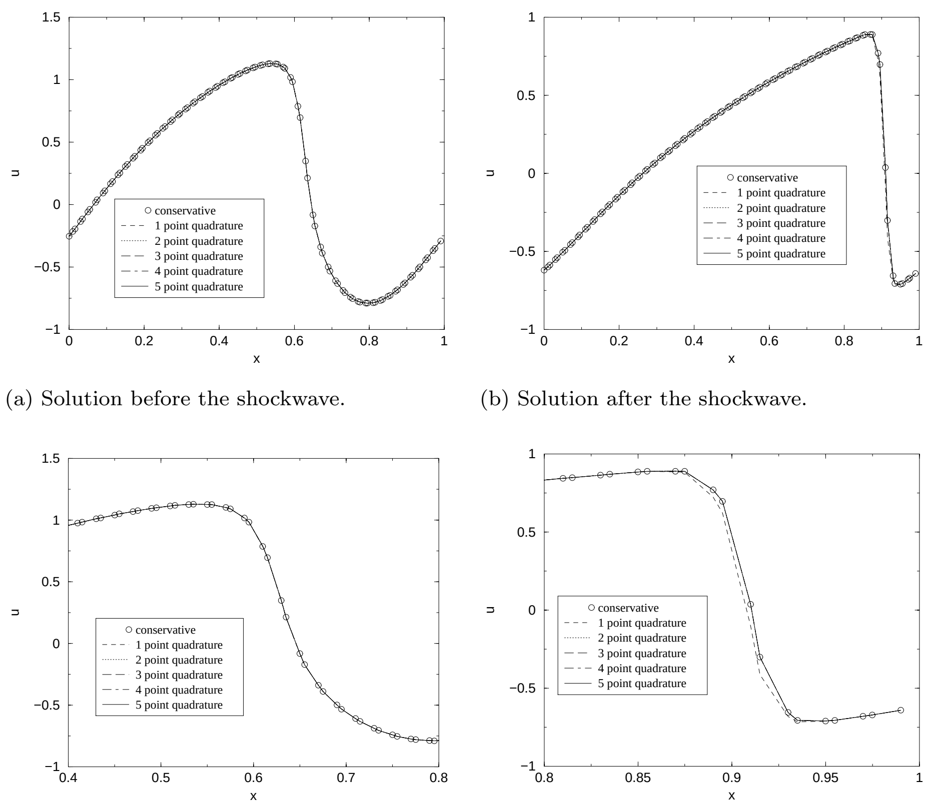

(a) Solution before the shockwave.

(b) Solution after the shockwave.

(c) Solution before the shockwave, zoom.

(d) Solution after the shockwave, zoom.

FIG. 7.1. *Numerical N-scheme solutions for* (1.1) *and* $u_i^0 = \sin(2\pi ih)$. *Solutions before the formation of a shockwave* ((a) *and* (c)) *and solutions after the formation of a shockwave* ((b) *and* (d)).

quadrature on a mesh containing 100 unknowns. All the solutions are virtually indistinguishable before the occurrence of the shockwave. It is only after the solution becomes discontinuous that the importance of sufficient-order Gauss quadrature is

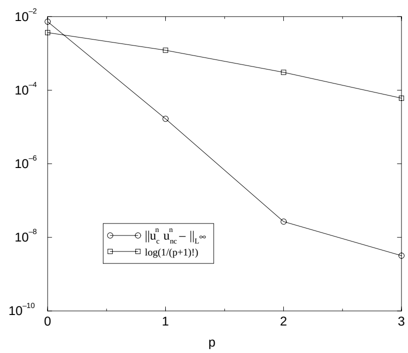

FIG. 7.2. *Comparison between* $\log\left(\frac{1}{(p+1)!}\right)$ *and* $||u_c^n - u_{nc}^n||_{L^\infty}$ *versus number of quadrature points for* $h = 0.625\ 10^{-3}$.

TABLE 7.2
Error between the conservative and adaptive quadrature schemes at $t = 0.5$ *using* 1, 2, *or* 3 *point Gauss quadrature.*

Mesh size, Δx	$L^1(u_{nc} - u_c)$	$L^2(u_{nc} - u_c)$	$L^\infty(u_{nc} - u_c)$	NQ_{min}	NQ_{max}
$0.100\ 10^{-1}$	$0.39005\ 10^{-4}$	$0.11351\ 10^{-3}$	$0.69521\ 10^{-3}$	1	2
$0.500\ 10^{-2}$	$0.27998\ 10^{-4}$	$0.13526\ 10^{-3}$	$0.12200\ 10^{-2}$	1	2
$0.250\ 10^{-2}$	$0.21424\ 10^{-4}$	$0.16100\ 10^{-3}$	$0.18236\ 10^{-2}$	1	2
$0.125\ 10^{-2}$	$0.18526\ 10^{-4}$	$0.20768\ 10^{-3}$	$0.36673\ 10^{-2}$	1	2
$0.100\ 10^{-1}$	$0.27007\ 10^{-4}$	$0.64119\ 10^{-4}$	$0.38681\ 10^{-3}$	1	3
$0.500\ 10^{-2}$	$0.13642\ 10^{-4}$	$0.52260\ 10^{-4}$	$0.47082\ 10^{-3}$	1	3
$0.250\ 10^{-2}$	$0.57902\ 10^{-5}$	$0.34398\ 10^{-4}$	$0.38955\ 10^{-3}$	1	3
$0.125\ 10^{-2}$	$0.22238\ 10^{-5}$	$0.20259\ 10^{-4}$	$0.35797\ 10^{-3}$	1	3

visually apparent and multiple quadrature points needed. The tabulated results reveal two effects addressed by the theory: (1) the L^1 error eventually stagnates when $h \to 0$ for fixed-order quadrature, and (2) the L^1 error decreases very rapidly with increasing NQ. In fact, upon closer inspection, this error decreases much more quickly than $(p+1)!$; see Figure 7.2.

7.1.2. 1-D numerical experiment: Adaptive Gauss quadrature on nonuniform mesh. The results of the previous 1-D numerical experiment of section 7.1.1 show very negligible sensitivity to the number of quadrature points whenever the solution is smooth. This observation suggests the following simple adaptive quadrature scheme, which uses a nondimensional measure of solution gradient to estimate solution smoothness:

- If $\frac{u_{i+1}-u_i}{\max(|u_i|,|u_{i+1}|)} \leq \sqrt{\Delta x/L}$, then the solution is smooth. Compute $\psi^+_{j+1/2}$ and $\psi^-_{j+1/2}$ with NQ_{min} point quadrature.
- Else, compute $\psi^+_{j+1/2}$ and $\psi^-_{j+1/2}$ with NQ_{max} point quadrature.

Repeating the calculations of section 7.1.1, Table 7.2 tabulates the corresponding numerical results using the adaptive parameters $NQ_{min} = 1$ and $NQ_{max} = 2, 3$ at the time $T = 0.5$ (after the formation of the shockwave). Note that, in these calculations, nearly all cells required only $NQ_{min} = 1$ quadrature points with only 3–5 cells requiring NQ_{max} number of quadrature points. This results in a notable savings in computational resources. These numerical results indicate that the quality of the solutions is comparable to the quality of those of Table 7.1 with some reduced accuracy that would be improved by a more stringent criterion for quadrature adaptation. We have not run this case with a second-order upwind scheme, but we believe that the same strategy could be used since quadrature with $NQ_{min} = 1$ points is second-order accurate. In fact, it can be shown formally that, to recover second-order accuracy, the "exact" total residual $\Phi^-_{j+1/2} + \Phi^+_{j+1/2}$ need only be recovered up to second-order accuracy to have a second-order accurate scheme; see [1]. Finally, we note that other tests have been carried out, for example, with the flux $f(u) = \exp(u^2)$, with similar results.

7.2. 2-D conservation laws. Next, we present 2-D solutions of the Euler equations of gasdynamics, assuming a perfect gas relationship. The significant computational savings obtained by adaptive numerical quadrature in 1-D suggest using a similar strategy in higher space dimensions, where the savings is even more dramatic. Throughout the remaining 2-D numerical experiments, standard quadrature formulas with positive weights for simplices [29] are utilized: 1 point $O(h^2)$ quadrature, 3 point $O(h^3)$ quadrature, 6 point $O(h^4)$ quadrature, 7 point $O(h^5)$ quadrature, and 16 point $O(h^7)$ quadrature. For any simplex T, a criterion must be developed which determines if the numerical solution is locally smooth. For efficiency, this decision should ideally be made from the information available in T only. Let s_j denote the (physical) entropy at node M_j and h_T denote the maximum length of the edges of T. We have implemented the following heuristic criterion for use in the adaptive quadrature strategy:

- If $\max_{M_i,M_j\in T} \left|\frac{s_i}{s_j} - 1\right| \leq \sqrt{h_T/L}$, then the solution is smooth. Compute the N-scheme decomposition using NQ_{min} point quadrature.
- Else, compute the N-scheme decomposition using NQ_{max} point quadrature.

7.2.1. 2-D numerical experiments: Euler equations on mesh triangulations. We first study the effect of the loss of conservation and the influence of the number of quadrature points for the N-scheme with quadrature. To do this, we select three test cases that are simple yet representative of different flow regimes: a subsonic flow test case, a transonic flow case with mild shockwaves, and a supersonic flow case over a blunt body, which produces a strong bow shockwave. The solutions are compared to those obtained by the reference conservative N-scheme using Z-variables. Our intent is not to assess the accuracy of the solution with respect to a mesh-converged solution, but rather to see how the loss of conservation affects the structure of the solution compared with the reference solution on the same mesh. In particular, we qualitatively and quantitatively compare the overall structure of conservative and nonconservative N-scheme solutions by examining representative cross-sectional and/or boundary data plots. Additionally, we examine the behavior of numerical solutions with adaptive mesh refinement for the cases containing discontinuities, where exact discrete conservation is normally very important, as it ensures proper solution jump approximation. Ideally, it would be illuminating to perform *uniform* mesh refinement in evaluating the adaptive quadrature N-scheme as $h \to 0$. This was done in the 1-D calculations. Unfortunately, this is prohibitively expensive in 2-D so we rely on multiple levels of adaptive mesh refinement to approximate the $h \to 0$ process.

7.2.2. Subsonic flow case. This case is taken from Dervieux et al. [9]. It is a flow over a cylinder with a Mach number at infinity of $M_\infty = 0.38$ computed on a relatively coarse mesh containing 3010 simplicial elements. Under these flow conditions, the flow remains subsonic and is devoid of solution discontinuities. Figures 7.3(a)–(d) show Mach number isolines for N-scheme calculations using 1, 3, and 7 point

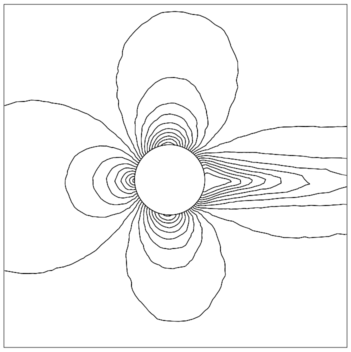

(a) 1 point quadrature

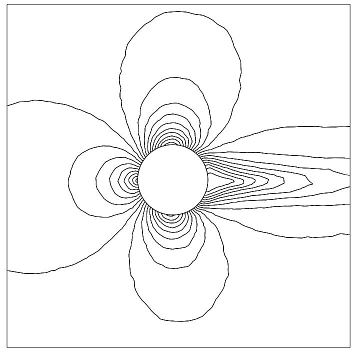

(b) 3 point quadrature

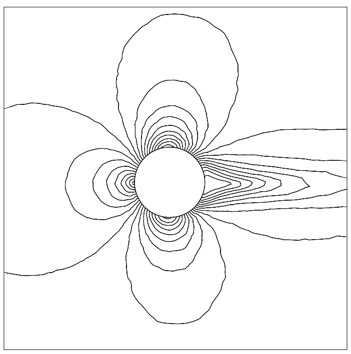

(c) 7 point quadrature

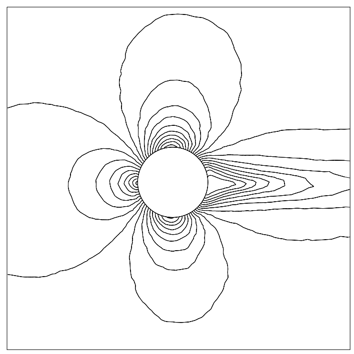

(d) conservative Z-variables

FIG. 7.3. (a)–(d) *Mach number isolines for N-scheme calculations using fixed* 1*,* 3*, and* 7 *point quadrature and the conservative Z-variables for the subsonic cylinder problem, $M_\infty = 0.38$, on a simplicial mesh containing* 3010 *elements.*

quadrature as well as the N-scheme using the conservative Z-variables. Figure 7.4(a) shows Mach number isolines for the N-scheme using the adaptive quadrature procedure described earlier with parameter values $NQ_{min} = 1$ and $NQ_{max} = 3$. Figure 7.4(b) provides a quantitative comparison of pressures on the surface of the cylinder using all the fixed and adaptive quadrature formulas as well as the conservative Z-variable N-scheme. As expected, all calculations show no discernible differences. These results confirm our analysis if we assume that the support of the measure μ is concentrated near discontinuities in the solution. Since there are no discontinuities in this flow, and our quadrature formulas are at least second-order accurate using single point quadrature, a Lax–Wendroff theorem is satisfied up to $O(h^2)$.

7.2.3. Transonic flow case. The second 2-D test case consists of transonic flow, $M_\infty = 0.85$, over the NACA0012 geometry with a flow incidence of 1 degree computed on a baseline simplicial mesh containing 5050 elements. The flow solution consists of both upper and lower surface shockwaves. Due to the 1 degree flow incidence, the upper surface shockwave is notably stronger than the lower surface shockwave. N-scheme calculations were performed using fixed 1, 3, and 7 quadrature point formulas as well as the conservative Z-variables on the baseline simplicial mesh. In addition, three levels of adaptive mesh refinement were performed and solutions computed using the adaptive quadrature N-scheme with $NQ_{min} = 1$ and $NQ_{max} = 3$. Surface

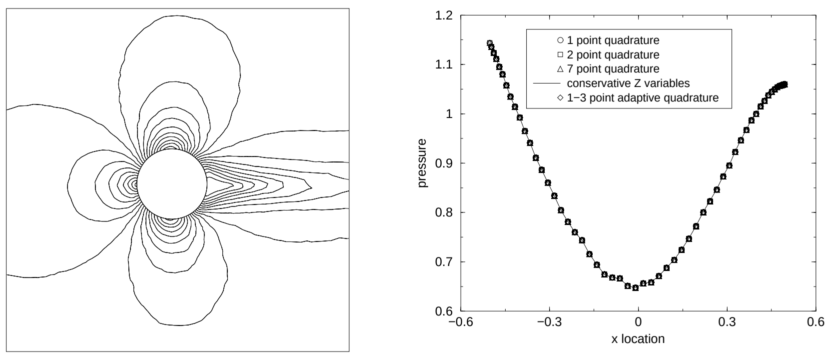

(a) 1–3 point adaptive quadrature (b) Pressure along top-bottom line of symmetry

FIG. 7.4. (a) *Mach number isolines for N-scheme calculations using* 1–3 *point adaptive quadrature and* (b) *the resulting pressure along top-bottom line of symmetry for the subsonic cylinder problem,* $M_\infty = 0.38$*, on a simplicial mesh containing* 3010 *elements.*

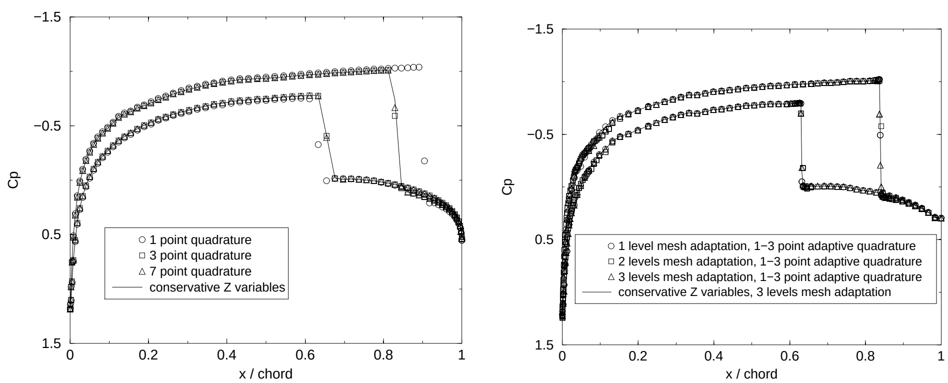

(a) Fixed 1, 3, and 7 point quadrature and conservative Z-variables

(b) Three levels of adaptive mesh refinement with 1–3 point adaptive quadrature

FIG. 7.5. *Surface pressure coefficient distribution on the NACA*0012 *airfoil using the N-scheme with* (a) 1*,* 3*, and* 7 *point quadrature and the conservative* Z*-variable, and* (b) *three levels of adaptive mesh refinement together with* 1–3 *point adaptive quadrature.*

pressure coefficient values are graphed in Figure 7.5(a) and Mach number isocontours shown in Figures 7.6(a)–(d) for N-scheme calculations using 1, 3, and 7 point quadrature and the conservative Z-variables. Similarly, surface pressure coefficient values are graphed in Figure 7.5(b) and Mach number isocontours in Figures 7.7(a)–(d) using three levels of shockwave-adapted mesh refinement together with the 1–3 point adaptive quadrature form of the N-scheme. Although the Mach number isocontour plots appear very similar, the Figure 7.5(a) graph of the pressure coefficient on the body of the NACA0012 airfoil is more revealing. This graph shows that the location of the shockwaves depends on the number of quadrature points. Specifically, the use of single point quadrature leads to a significant change in shockwave location when compared to 3 and 7 point quadrature as well as to the conservative Z-variable scheme. For this particular flow, the effect of the measure μ is not sufficiently reduced using one quadrature point, but using three or more quadrature points seems sufficient to reduce conservation error less than truncation errors present in the conservative N-scheme.

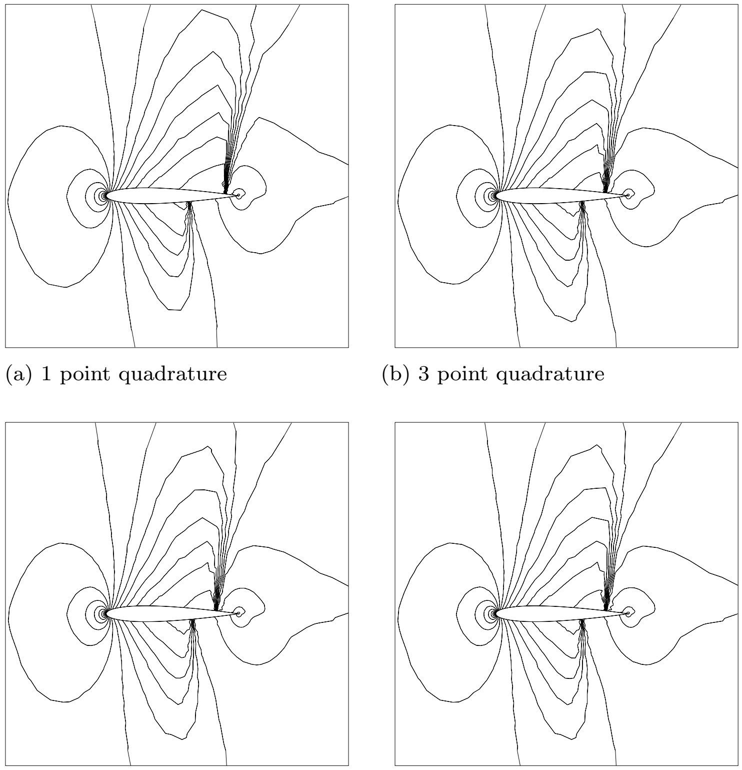

(a) 1 point quadrature (b) 3 point quadrature

(c) 7 point quadrature (d) Conservative Z-variables

FIG. 7.6. (a)–(d) *Mach number isolines for N-scheme calculation using fixed* 1, 3, *and* 7 *point quadrature and the conservative Z-variables for the transonic NACA*0012 *problem,* $M_\infty = 0.85$ *and* 1 *degree flow incidence, on a simplicial mesh containing* 5050 *elements.*

The comparability of the 3 and 7 point quadrature with the conservative Z-variable scheme once again suggests an adaptive quadrature implementation. The calculations presented in Figure 7.5(b) are intended to check whether the errors generated by the loss of conservation on refined meshes dominate the truncation error, even in an adaptive quadrature setting. With adaptive mesh refinement, all the computations in Figure 7.5(b) are very comparable, which further validates Theorem 3.1 and our adaptive quadrature strategy.

7.2.4. Supersonic blunt body flow. The last 2-D test case consists of supersonic flow, $M_\infty = 3.5$, over a circular cylinder geometry computed on a baseline simplicial mesh containing 4075 elements. The flow solution consists of strong bow shock forward of the cylinder geometry. Figures 7.8 (a)–(d) show Mach number isocontours for numerical solutions computed using 1, 3, and 7 point quadrature and conservative Z-variable forms of the N-scheme. In addition, Mach number isocontours for 1–3 and 1–7 point adaptive quadrature N-scheme calculations are shown in Figures 7.9 (a)–(b). Both fixed and adaptive quadrature calculations are compared in Figure 7.9 for pressure data along the top-bottom line of symmetry. This latter figure shows a large difference between the one quadrature calculation and the other calculations. This difference is also clearly seen in the Mach number isocontour plot, Figure 7.8(a). Perhaps, more importantly, Figure 7.9 shows that the 3 point

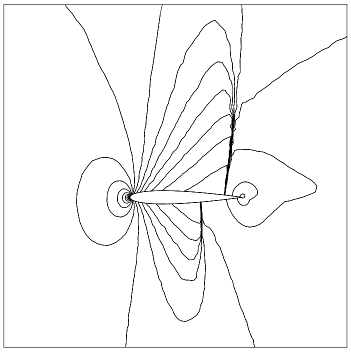

(a) 1 level adaptive mesh refinement, 1–3 point adaptive quadrature

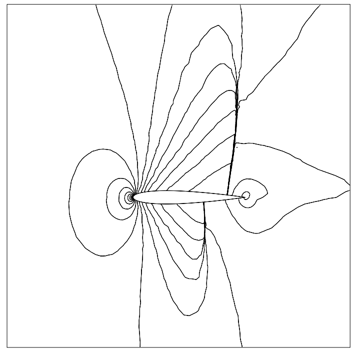

(b) 2 levels adaptive mesh refinement, 1–3 point adaptive quadrature

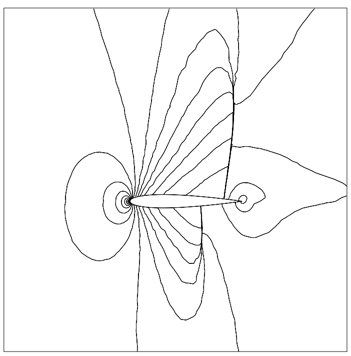

(a) 3 levels of adaptive mesh refinement, 1–3 point adaptive quadrature

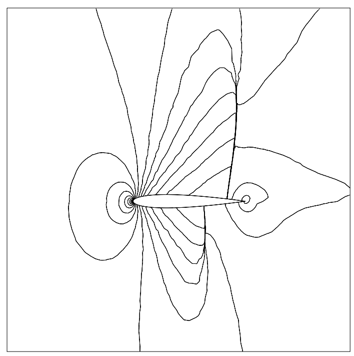

(b) 3 levels of adaptive mesh refinement, conservative Z-variables

Fig. 7.7. (a)–(d) *Mach number isolines for N-scheme calculations using* 1, 2, *and* 3 *levels of adaptive mesh refinement and* 1–3 *point adaptive quadrature and the reference conservative Z-variables on the* 3 *level refined mesh for the transonic $NACA0012$ problem $M_\infty = 0.85$ and* 1 *degree flow incidence.*

quadrature (and 1–3 point adaptive quadrature) also produced incorrect shockwave locations on the baseline mesh, although the error is much smaller than that obtained using 1 point quadrature. Recall that for the transonic flow problem, 3 point quadrature was of sufficient order on the baseline and adaptively refined meshes for computing correct shock locations. Using 7 point fixed quadrature and 1–7 point adaptive quadrature yields solution shockwave positions in agreement with the conservative scheme. These results are also in agreement with inequality (3.8) of Theorem 3.1, since the strength of the measure depends not only on the number of quadrature points but also on the supremum of a norm of higher derivatives of the flux, $D^{k+1}_{\mathbf{v}}\mathbf{f}_{,\mathbf{v}}$. Estimation of this norm is difficult, but it is reasonable that this number tends to infinity as the maximum Mach number also tends to ∞. However, since the flux $\mathbf{f}$ is analytical in $\mathbf{v}$ and the Mach number is finite, the right-hand side of (3.8) still converges to zero, albeit more slowly.

Next, we examine the effect of adaptive mesh refinement. Figures 7.10(a)–(c) show Mach number isocontours for the N-scheme calculations using 16 point quadrature, 1–16 point adaptive quadrature, and conservative Z-variables. Figure 7.10(d) shows a graph of Mach number along the top-bottom line of symmetry for these same

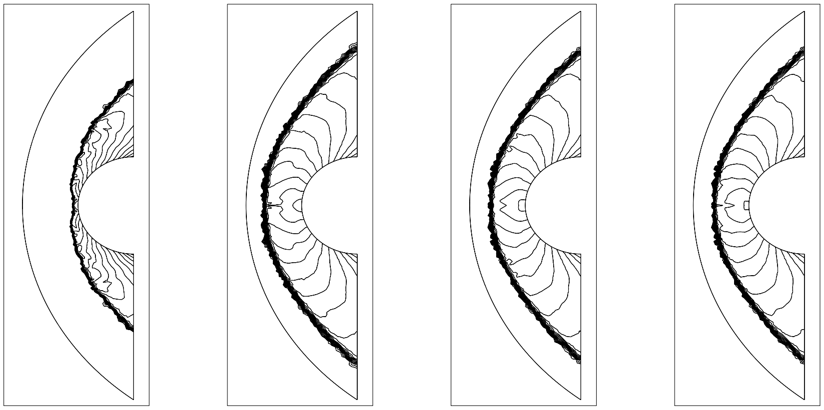

(a) 1 point quadrature (b) 3 point quadrature (c) 7 point quadrature (d) conservative Z-variables

FIG. 7.8. *Mach number isolines for N-scheme calculations using fixed* 1, 3, *and* 7 *point quadrature and the conservative* Z*-variables for the supersonic cylinder problem,* $M_\infty = 3.5$ *on the baseline simplicial mesh containing* 4075 *elements.*

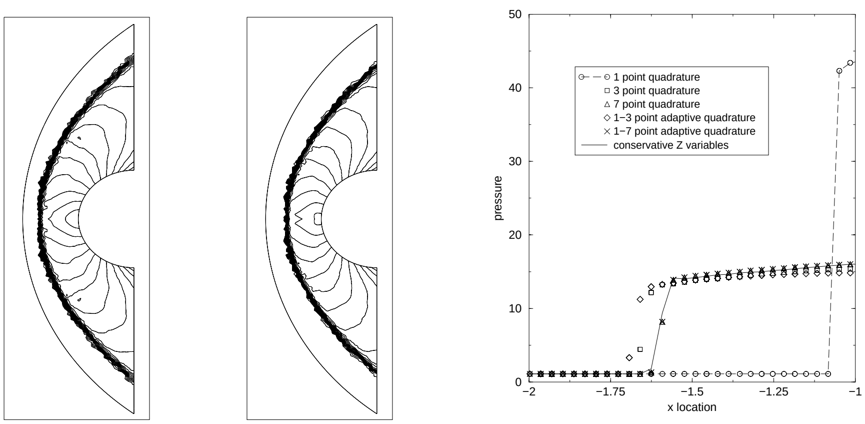

(a) 1–3 point adaptive quadrature (b) 1–7 point adaptive quadrature (c) Pressure along top-bottom line of symmetry

FIG. 7.9. (a)–(b) *Mach number isolines for N-scheme calculations using* 1–3 *and* 1–7 *point adaptive quadrature, and* (c) *comparison of all fixed and adaptive quadrature N-scheme calculations along the top-bottom line of symmetry for the supersonic cylinder problem,* $M_\infty = 3.5$ *on the baseline simplicial mesh containing* 4075 *elements.*

schemes as well as 1–7 point adaptive quadrature. Surprisingly, this figure shows small differences in shock profile using 1–7 point adaptive quadrature for this problem with three levels of adaptive mesh refinement. It is only with 16 point fixed or adaptive quadrature that the adaptive N-scheme solutions match the conservative Z-variable N-scheme. This demonstrates some slight dependency on the mesh parameter h not captured by the present analysis.

8. Concluding remarks. A number of upwind schemes are derived in quasilinear form and discrete conservation obtained by devising specialized mean-value linearized coefficients. This approach is problematic for systems such as magnetohydrodynamics, Euler equations with certain forms of chemistry, etc., where these

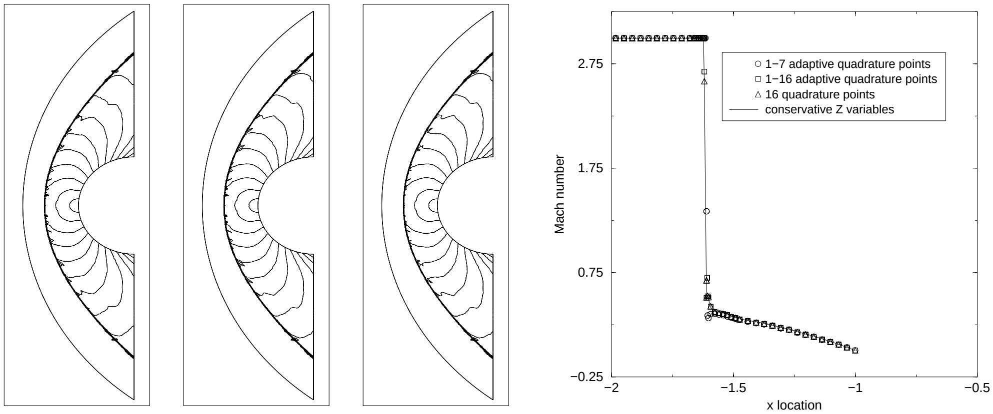

(a) 16 point quadrature (b) 1–16 point quadrature (c) conservative Z-variables (d) symmetry line Mach number plot

FIG. 7.10. (a)–(b) *Mach number isolines for N-scheme calculations using* 16 *point fixed and* 1–16 *point adaptive quadrature, and* (c) *conservative Z-variables for the supersonic cylinder problem.* (d) *Comparison of Mach number on top-bottom symmetry line, $M_\infty = 3.5$, on the baseline simplicial mesh with* 3 *levels of adaptive mesh refinement.*

specialized mean-value linearizations may not exist in closed form. In the present analysis, we consider a more general construction of these upwind schemes that avoids explicitly constructing these exact mean-value linearizations. Our construction is well tailored to systems of conservation laws with convex entropy extension. Using the tools of weak convergence, a Lax–Wendroff theorem has been derived for this class of nonconservative schemes utilizing numerical quadrature. By using sufficient-order numerical quadrature, we show that correct weak solutions of conservation laws are obtained. Numerical results confirm the basic analysis but do show some weak interdependence of the mesh space parameter h and the required order of accuracy of the numerical quadrature. This indicates that further investigation and quantification of this effect are needed.

Acknowledgment. The authors thank Katherine Mer-Nkonga of the French Atomic Commission for all the suggestions she has given to complete section 3.

REFERENCES

[1] R. ABGRALL, *Toward the ultimate conservative scheme: Following the quest*, J. Comput. Phys., 167 (2001), pp. 277–315.

[2] R. ABGRALL AND K. MER, *Un théorème de type Lax–Wendroff pour les schémas distributifs*, Technical report 98010, Mathématiques Appliquées de Bordeaux, Université Bordeaux, Talence, France, 1998.

[3] O. AXELSSON, *Iterative Solution Methods*, Cambridge University Press, Cambridge, UK, 1996.

[4] T. J. BARTH, *Simplified discontinuous Galerkin methods for systems of conservation laws with convex extension*, in Proceedings of the 1st International Conference on Discontinuous Galerkin Methods, Lecture Notes in Comput. Sci. Engrg. II, B. Cockburn, G. E. Karniadakis, and C.-H. Shu, eds., Springer, Berlin, 2001, pp. 63–75.

[5] T. J. BARTH, *Some Working Notes on Energy Analysis of the Matrix N-scheme*, NASA Ames Research Center, Moffett Field, CA, 1996.

[6] T. J. BARTH, *Numerical methods for gasdynamic systems on unstructured meshes*, in An Introduction to Recent Developments in Theory and Numerics for Conservation Laws, Lecture Notes in Comput. Sci. Engrg. 5, D. Kröner, M. Ohlberger, and C. Rohde, eds., Springer-Verlag, Heidelberg, 1998, pp. 195–285.

[7] P. I. Crumpton, J. A. MacKenzie, and K. W. Morton, *Cell vertex algorithms for the compressible Navier-Stokes equations*, J. Comput. Phys., 109 (1993), pp. 1–15.

[8] H. Deconinck, R. Struijs, and P. L. Roe, *Compact Advection Schemes on Unstructured Grids*, von Karman Institute Lecture Series Monograph 1993-04, von Karman Institute for Fluid Dynamics, Belgium, 1993.

[9] A. Dervieux, B. van Leer, J. Périaux, and A. Rizzi, eds., *Numerical Simulation of Compressible Euler Flows*, Notes on Numerical Fluid Mechanics 26, Friedr. Vieweg & Sohn, Braunschweig, 1989.

[10] S. K. Godunov, *A finite difference method for the numerical computation of discontinuous solutions of the equations of fluid dynamics*, Mat. Sb., 47 (1959), pp. 271–306.

[11] S. K. Godunov, *An interesting class of quasilinear systems*, Dokl. Akad. Nauk. SSSR, 139 (1961), pp. 521–523.

[12] G. Golub, *Private communication,* Stanford University, Stanford, CA, March 11, 1996.

[13] A. Harten, P. D. Lax, and B. van Leer, *On upstream differencing and Godunov-type schemes for hyperbolic conservation laws*, SIAM Rev., 25 (1983), pp. 35–61.

[14] T. Y. Hou and P. G. Le Floch, *Why nonconservative schemes converge to wrong solutions: Error analysis*, Math. Comp., 62 (1994), pp. 497–530.

[15] T. J. R. Hughes, L. P. Franca, and M. Mallet, *A new finite element formulation for CFD:* I. *Symmetric forms of the compressible Euler and Navier-Stokes equations and the second law of thermodynamics*, Comput. Methods Appl. Mech. Engrg., 54 (1986), pp. 223–234.

[16] T. J. R. Hughes and M. Mallet, *A new finite element formulation for CFD:* III. *The generalized streamline operator for multidimensional advective-diffusive systems*, Comput. Methods Appl. Mech. Engrg., 58 (1986), pp. 305–328.

[17] C. Johnson, *Numerical Solution of Partial Differential Equations by the Finite Element Method*, Cambridge University Press, Cambridge, UK, 1987.

[18] C. Johnson and A. Szepessy, *Convergence of the shock-capturing streamline diffusion finite element methods for hyperbolic conservation laws*, Math. Comp., 54 (1990), pp. 107–129.

[19] D. Kröner, *Numerical Schemes for Conservation Laws*, John Wiley and B. G. Teubner, New York, 1997.

[20] D. Kröner, M. Rokyta, and M. Wierse, *A Lax-Wendroff type theorem for upwind finite volume schemes in* 2-*d*, East-West J. Numer. Math., 4 (1996), pp. 279–292.

[21] P. Lax and B. Wendroff, *Systems of conservation laws*, Comm. Pure Appl. Math., 13 (1960), pp. 217–237.

[22] P. D. Lax, *Hyperbolic Systems of Conservation Laws and the Mathematical Theory of Shock Waves*, SIAM, Philadelphia, 1973.

[23] M. S. Mock, *Systems of conservation laws of mixed type*, J. Differential Equations, 37 (1980), pp. 70–88.

[24] K. W. Morton and E. Süli, *Finite volume methods and their analysis*, IMA J. Numer. Anal., 11 (1991), pp. 241–260.

[25] R.-H. Ni, *A multiple grid scheme for solving the Euler equations*, AIAA J., 20 (1981), pp. 1565–1571.

[26] P. L. Roe, *Approximate Riemann solvers, parameter vectors, and difference schemes*, J. Comput. Phys., 43 (1981), pp. 357–372.

[27] P. L. Roe, *Linear Advection Schemes on Triangular Meshes*, Technical Report CoA 8720, Cranfield Institute of Bioscience and Technology, Cranfield University, Bedforshire, UK, 1987.

[28] P. L. Roe, *"Optimum" Upwind Advection on a Triangular Mesh*, Technical report, ICASE, NASA Langley Research Center, 1990.

[29] G. Strang and G. J. Fix, *An Analysis of the Finite Element Method*, Prentice-Hall, Englewood Cliffs, NJ, 1973.

[30] R. Struijs, H. Deconinck, and P. L. Roe, *A multidimensional generalization of Roe's flux difference splitter for the euler equations*, Comput. Fluids, 22 (1993), pp. 215–222.

[31] E. van der Weide and H. Deconinck, *Positive matrix distribution schemes for hyperbolic systems*, in Computational Fluid Dynamics '96, Wiley, New York 1996, pp. 747–753.

[32] B. van Leer, *Towards the ultimate conservative difference schemes* V. *A second-order sequel to Godunov's method*, J. Comput. Phys., 32 (1979), pp. 101–136.